Vortex-Wave Dynamics in the Drift Wave-Rossby Wave Problem with Temperature Gradients

W. Horton
Institute for Fusion Studies
The University of Texas at Austin, Austin, TX 78712

August, 1997

Abstract

The processes governing the propagation of low frequency vortex-wave convective disturbances in the two different physical systems of neutral fluids on rotating planets and plasmas confined by magnetic fields are explored with (i) physical descriptions of the convective transport, (ii) establishing the relevant conservation laws and (iii) computer simulations. The role of a global, ambient temperature gradient in driving the three-dimensional baroclinic instability is compared with the ion temperature gradient instability in magnetically confined plasma. Steady-state power balance and the turbulent viscosities and thermal diffusivities are analyzed using the same class of turbulent transport formulas.

Contents

1 Drift Waves–Rossby Waves

There are important similarities in the geophysical fluid dynamics and the low frequency drift wave dynamics in magnetized plasmas. In both systems the motions are quasi-two-dimensional, meaning that there are large horizontal velocities $\mathbf{v}_\perp$ that can often be taken nearly independent of the vertical coordinate z or the direction parallel to the magnetic field in the plasma. The fundamental reason for the similar structure of the low-frequency dynamics in the two systems with completely different physical properties, neutral fluids versus the charged particle system, is the mathematical form of the horizontal acceleration. In a fluid system rotating with angular velocity $\mathbf{\Omega}$ the Coriolis force $2\rho\mathbf{v}\times\mathbf{\Omega}$ where ρ is the mass density, has exactly the same mathematical form as the Lorentz force $e_a n_a \mathbf{v}_a \times \mathbf{B}/c$ acting on the charged fluid with a cyclotron frequency $\mathbf{\Omega}_a = e_a\,\mathbf{B}/m_a\,c$ for charge species e_a, m_a with density n_a and pressure $p_a = n_a k_B T_a$.

The degree of the correspondence of the two systems is made precise by establishing the form of the potential vorticity $q(x,y,t)$ in the two systems and the form of Ertel's theorem $dq/dt = 0$. The parallel between the drift wave dynamics and the geophysical fluid dynamics was first emphasized by Hasegawa and Mima (1978), Hasegawa *et al.* (1979). The homology is clarified through the use of Ertel's theorem by Meiss and Horton (1983). Meiss and Horton introduce the name Charney-Hasegawa-Mima (CHM) equation to describe the isomorphism between the two systems that occurs in the strictly 2D limit where the Taylor-Proudman theorem holds in the strong sense. Meiss and Horton (1983) also describe the generalization of the system to include the motion parallel to the rotation axis. When the coupling to the vertical velocity $w(v_\parallel)$ is important the GFD and plasma dynamics begin to differ due to the stable stratification from the buoyancy effects in the atmosphere and oceans. To the extent that the stratification dynamics given by the Brunt-Väisälä frequency N is rapid compared to the Coriolis frequency parameter $f = 2\Omega\sin\theta$ where θ is the latitude ($N \gg f$)

the net effect of the stratification on the long-time scale $T > 1/f$ dynamics is to maintain the quasi-two-dimensionality of the large-scale ($L > \rho_R$) dynamics. Here ρ_R is the Rossby radius measuring the horizontal scale for dispersion of the Rossby waves and the exponential decay length for localized vortex structures. The effect of the vertical stratification is to decrease the effective Rossby radius from the shallow water value $\rho_R = (gH)^{1/2}/f$ to the internal deformation radius $\rho_I = NH/f$. The origin of this change in the Rossby radius due to the vertical stratification of the fluid is explained in the section on vertical motion in stratified medium.

In Sec. 2 we introduce the instabilities that occur from the horizontal temperature gradient. In the GFD system this instability is called the baroclinic instability and is perhaps the most important and universal form of instability in the atmosphere (Gill, 1982, ch. 13). The fastest growth rate occurs for the horizontal wavenumber $k_\perp$ such that the $k_\perp \rho_R \sim 1$ (Pedlosky, 1987, p. 521) which for $\rho_R = 1000\,\mathrm{km}$ gives the azimuthal mode number $m = 6$ for the Earth. Monin (1972) attributes the peak in the power spectrum of the kinetic energy fluctuations at the period of four days to this source of turbulence. These facts are similar to the situation in confined plasmas when appropriately scaled. The ion temperature gradient instability (Horton *et al.*, 1980, 1981, and 1992) has a peak in the wavenumber spectrum at $k_\perp \rho_s \sim 0.3$ with $\omega/\Omega_i \simeq 0.3\rho_s/L_T$. Here Ω_i is the ion cyclotron frequency and $\rho_s = c_s/\Omega_i$ is the ion inertial scale length which are the plasma analogs of f and ρ_R as shown in Table 1. The scale length of the radial temperature gradient is L_T. Examples of the large-scale quasi-two-dimensional convection cells obtained from direct numerical simulations are presented.

We conclude in Sec. 3 by comparing the turbulent thermal transport problem for the atmosphere and the plasma. We discuss the alternative scaling laws for the effective thermal diffusivity χ. Arguments are given to show that both for the atmosphere and the plasma the Prandtl number constructed from the ratio of the large-scale turbulent viscosity ($L >$

Table 1: Analogy Between Drift Wave and Rossby Wave

Drift Wave	**Rossby Wave**
H-M equation: $(1-\nabla^2)\frac{\partial \phi}{\partial t} + v_d \frac{\partial \phi}{\partial y} - [\phi, \nabla^2 \phi] = 0$	Charney equation: $(1-\nabla^2)\frac{\partial h}{\partial t} - v_R \frac{\partial h}{\partial x} - [h, \nabla^2 h] = 0$
Electrostatic potential $\phi(x,y,t)$ $\phi(x,y,t) = \left(\frac{L_n}{\rho_s}\right) e\Phi\left(\frac{x}{\rho_s}, \frac{y}{\rho_s}, \frac{c_s}{r_n}\, t\right) \Big/ T_e$	Variable part of fluid depth: $h(x,y,t)$ $h(x,y,t) = \left(\frac{L_R}{\rho_g}\right) \delta H\left(\frac{x}{\rho_g}, \frac{y}{\rho_g}, \frac{c_g}{L_R}\, t\right) \Big/ H$
Lorentz force: $m_i\, \omega_{ci}\, \mathbf{v}_\perp \times \widehat{\mathbf{z}}$	Coriolis force: $\rho f \mathbf{v}_\perp \times \widehat{\mathbf{z}}$
$\mathbf{E} \times \mathbf{B}$ drift flow: $\mathbf{v}_\perp = \left(\frac{c}{B}\right) \widehat{\mathbf{z}} \times \boldsymbol{\nabla} \Phi$	Geostrophic flow: $\mathbf{v}_\perp = \left(\frac{g}{f}\right) \widehat{\mathbf{z}} \times \boldsymbol{\nabla} \delta H$
Cyclotron frequency: $\omega_{ci} = \frac{eB}{cm_i}$	Coriolis parameter: f
Drift coefficient: $L_n^{-1} = -\frac{\partial}{\partial x}\, \ell n\, n_0$	Rossby coefficient: $L_R^{-1} = \frac{\partial}{\partial y}\, \ell n \left(\frac{f}{H}\right)$
Larmor radius: $\rho_s = \frac{c_s}{\omega_{ci}}$	Rossby radius: $\rho_g = \frac{c_g}{f}$
Ion acoustic speed: $c_s = \left(\frac{T_e}{m_i}\right)^{1/2}$ where T_e is electron temperature	Gravity wave speed: $c_g = (gH)^{1/2}$ where H is depth of fluid layer.
Drift velocity: $v_d = c_s\, \rho_s\, \frac{\partial}{\partial x}\, \ell n\, n_0$	Rossby velocity: $v_R = c_g\, \rho_g\, \frac{\partial}{\partial y}\, \ell n \left(\frac{f}{H}\right)$
Dispersion relation: $\omega = \frac{k_y\, v_d}{1+k^2\, \rho_s^2}$	Dispersion relation: $\omega = -\frac{k_x\, v_R}{1+k^2\, \rho_g^2}$

1000 km using the Richardson four-thirds law) and the turbulent thermal diffusivity χ is comparable to unity.

1.1 Physical mechanism of the drift wave–Rossby wave

With Fig. 1 showing the positive potential associated with a local excess of positive charge, we can understand the drift wave propagation from the convection of the ion density. The convection of the plasma density is given by

$$\frac{\partial n}{\partial t} + \mathbf{v}_E \cdot \boldsymbol{\nabla} n = 0 \tag{1}$$

where

$$\mathbf{v}_E = \frac{c\mathbf{E} \times \mathbf{B}}{B^2} = \frac{c\widehat{\mathbf{z}} \times \nabla \Phi}{B}. \tag{2}$$

Clearly the flow (2) is along the contours of constant electric potential Φ and from Eq. (1) the higher density at the top of the frame is brought to the right and the lower density beneath the structure is brought to the left. In time Δt the amount of excess density δn that accumulates to the right of the potential maximum Φ is $\delta n \Delta x \Delta y = (n_> \mathbf{v}_E - n_< \mathbf{v}_E) \cdot \widehat{\mathbf{x}} \Delta y \Delta t$. The electron fluid is able to move freely and rapidly along the magnetic field $\mathbf{B}$ to neutralize

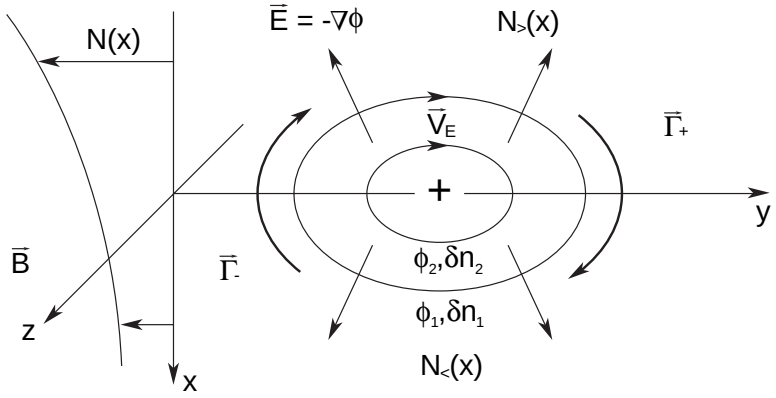

Figure 1: Drift wave mechanism showing $\mathbf{E} \times \mathbf{B}$ convection in a nonuniform, magnetized plasma. The local potential maximum Φ produces clockwise rotation that moves the structure to the right with the speed given in Eq. (4)..

the excess charge $n_i = n_e(x)\exp(e\Phi/T_e) \simeq n_0(1 + e\Phi/T_e)$ for small $\varphi = e\Phi/T_e$. Combining these results for δn with the flow through the midplane

$$\mathbf{v}_E \cdot \widehat{\mathbf{x}} \Delta y = cE_y \Delta y/B = c\Phi/B \tag{3}$$

and the density excess

$$n_> - n_< = \Delta x \, \partial n/\partial x$$

gives that the potential maximum Φ moves to the position $y + \Delta y$ at the speed

$$\frac{\Delta y}{\Delta t} = \frac{-cT_e}{eBn} \frac{\partial n}{\partial x} = v_{de}. \tag{4}$$

Even with constant n the structure will translate when $v_E^> \neq v_E^<$ due to $\Delta x \partial B/\partial x$. This is the basic mechanism of the plasma drift wave.

For an incompressible fluid of depth $H(x, y, t)$ the hydrostatic pressure is $p = \rho g H(x, y, t)$ and the geostrophic flow velocity balances the pressure gradient $-\nabla p + \rho f \mathbf{v} \times \widehat{\mathbf{z}} = 0$ to give

$$\mathbf{v} = \frac{g}{f} \widehat{\mathbf{z}} \times \nabla H. \tag{5}$$

Now reconsider Fig. 1 with depth of the fluid $H_0(x)$ corresponding to the density $n(x)$. The local potential Φ now corresponds to the excess column height $g\delta H(x, y, t)$ of an anticyclone. Again there is clockwise rotation bringing the deeper fluid to the right and the shallow water to the left so that the bulge $\delta H > 0$ propagates to the right with the speed $v_R = (g/f)(\partial H/\partial x)$. Reversing the sign of the perturbation $\delta H < 0$ changes the direction of rotation for the low pressure cyclone. However, the depression again moves to the right with the same speed since the counter clockwise rotation brings shallower fluid to the right. For nonlinear finite amplitude disturbances $h = \delta H/H$ the deeper anticyclonic perturbation propagates faster than the cyclonic disturbance.

The dynamical equation for $H(x, y, t)$ follows from integrating the incompressibility condition

$$\nabla \cdot \mathbf{v}_\perp + \frac{\partial w}{\partial z} = 0 \tag{6}$$

from $z = H_B(x,y)$ the bottom to $z = H(x,y,t) + H_B$ the free surface and using that $w(z = H_B) \equiv 0$ and $w(z = H + H_B) = dH/dt$ while taking $\mathbf{v} = u\widehat{\mathbf{x}} + v\widehat{\mathbf{y}}$ independent of z (Pedlosky, 1987, p. 62). The shallow water equation is then

$$\frac{\partial H}{\partial t} + \mathbf{v}_\perp \cdot \nabla H + H \nabla \cdot \mathbf{v}_\perp = 0. \tag{7}$$

Using the geostrophic velocity with $f = f(y)$ and $H = H_0(y)$ as in the standard GFD coordinates, we obtain

$$\frac{\partial}{\partial t}\,\delta H + g\,\frac{\partial}{\partial y}\left(\frac{H_0(y)}{f(y)}\right)\frac{\partial \delta H}{\partial x} = 0 \tag{8}$$

for the long wavelength Rossby wave equation. Note that y points northward and x eastward with the Rossby wave propagating westward. The fusion coordinates in Fig. 1 are obtained by rotating the GFD coordinates anticlockwise about $\widehat{\mathbf{z}}$ by 90° so that the $\widehat{\mathbf{x}}$ points in the direction of the decreasing density $n(x)$ and $\widehat{\mathbf{y}}$ in the direction of the drift wave propagation. The simulations presented here are expressed in terms of the fusion coordinates while we leave the GFD equations in GFD coordinates.

In the presence of resistivity or the electron Landau resonance the density and potential fluctuations develop a phase difference as shown in Fig. 2. Repeating the above argument with the phase difference shows that there is now a net transport from $\langle n\mathbf{v}_E \cdot \widehat{\mathbf{x}}\rangle_y$ and that there is a growth or decay of the amplitude of the structure depending on the direction of the phase shift. The same situation will arise in Sec. 2 for the phase of the temperature fluctuation relative to that of the stream function for the $\mathbf{v}_\perp$ flow velocity. For unstable fluctuations the net transport is down the relevant density or temperature gradient which determines the direction of the phase shift between the stream function and the transported field. For large amplitude, coherent structures the phase shift tends to be small.

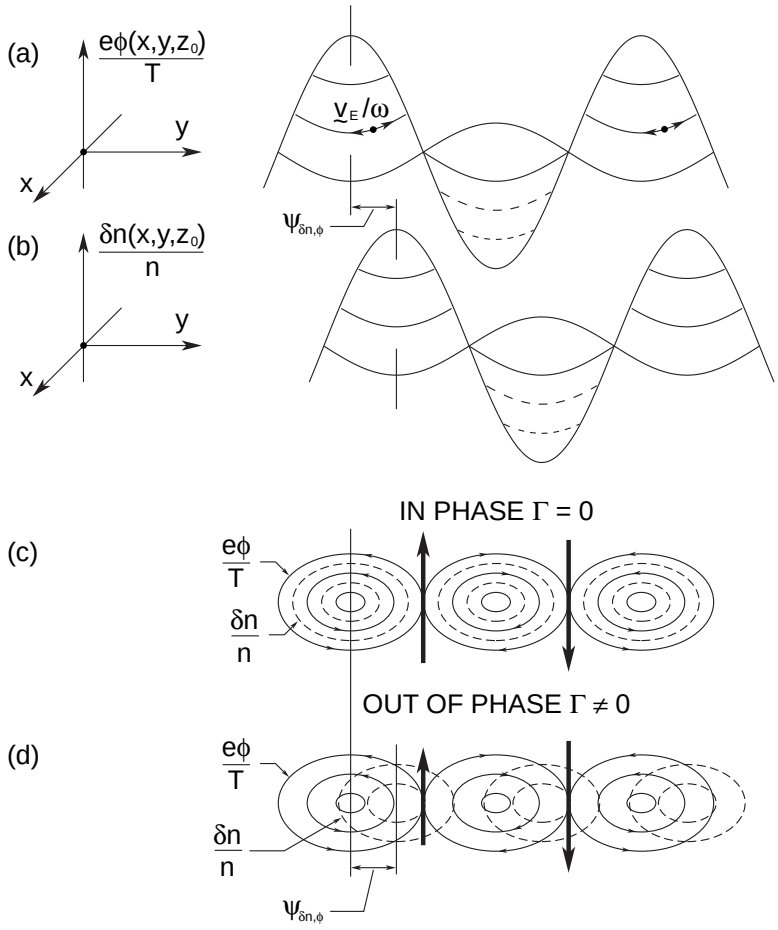

Figure 2: (a) A segment of a drift wave fluctuation showing the variation of the electrostatic potential perpendicular to the magnetic field at a given instant of time. The isopotential contours in the plane perpendicular to $B\hat{\mathbf{z}}$ are the stream lines of the $\mathbf{E} \times \mathbf{B}$ particle motion. (b) A segment of the correlated but phase shifted density variation. (c) Top view of the potential and density contours in (a) and (b) in the case where the density and potential variation are in phase. (d) Top view in the case where the potential and density variation are out of phase by $\psi_{\delta n,\varphi}$.

1.2 Ertel's theorem

The isomorphism between the drift wave and the Rossby wave is most clearly and usefully expressed by Ertel's theorem in the reduced form suitable for geostrophic and $\mathbf{E} \times \mathbf{B}$ flows. To see the action of the Coriolis force/Lorentz force in keeping the variation of $\mathbf{v}_\perp$ small with z, it is useful to examine the rotational part first for the full 3D momentum equation and then afterwards consider the rotational and the divergence parts of the horizontal components of the acceleration equation separated from the vertical component. The full 3D acceleration equation is

$$\rho \frac{d\mathbf{v}}{dt} = -\nabla p + \rho \mathbf{v} \times \mathbf{f} + \rho \mathbf{g}. \tag{9}$$

Upon using the vector identity

$$\mathbf{v} \cdot \nabla \mathbf{v} = \nabla \left(\frac{v^2}{2} \right) - \mathbf{v} \times (\nabla \times \mathbf{v}) \tag{10}$$

to rewrite the convective derivative we see that the effective pressure is the sum of the thermal pressure and the dynamic pressure $p_{\text{eff}} = p + \rho v^2$ and the horizontal rotational acceleration becomes $\mathbf{v} \times (f + \boldsymbol{\nabla} \times \mathbf{v})$ where $\boldsymbol{\omega} = \nabla \times \mathbf{v}$ the vorticity in the rotating frame combines with $\mathbf{f}$ to give the absolute vorticity $\mathbf{f} + \boldsymbol{\omega}$.

Dividing Eq. (9) by the mass density and taking the rotational part yields

$$\frac{d}{dt}(\boldsymbol{\omega} + \mathbf{f}) = (\boldsymbol{\omega} + \mathbf{f}) \cdot \nabla \mathbf{v} - (\boldsymbol{\omega} + \mathbf{f})(\nabla \cdot \mathbf{v}) + \frac{\nabla \rho \times \nabla p}{\rho^2} \tag{11}$$

for the convection of the absolute vorticity. Equation (11) shows that in the rotating frame the absolute vorticity $\mathbf{f} + \boldsymbol{\omega}$ plays the same role as $\boldsymbol{\omega}$ in an inertial frame.

For $p = p(\rho)$ the last term in Eq. (11) vanishes and the alternative form of Eq. (11) familiar to plasma physicists is

$$\partial_t(\boldsymbol{\omega} + \mathbf{f}) = \nabla \times [\mathbf{v} \times (\boldsymbol{\omega} + \mathbf{f})] .$$

This is the same as the "frozen in law" for the magnetic flux $\int \mathbf{B} \cdot d\mathbf{a}$ in the limit of infinite conductivity. Thus, the corresponding flux $\int_S (\boldsymbol{\omega} + \mathbf{f}) \cdot d\mathbf{a}$ through a surface S moving with the

fluid velocity $\mathbf{v}(\mathbf{x}, t)$ is constant. This is the general form of the Taylor-Proudman theorem according to Chandrasekhar (1961, p. 84).

The Taylor-Proudman theorem states that for stationary, incompressible flow with $\nabla p \times \nabla \rho = 0$ the flow velocity $\mathbf{v}$ is independent of the z. The first term on the right-hand side of Eq. (11) gives the differential form of the Taylor-Proudman theorem: $\mathbf{f} \cdot \nabla \mathbf{v} = 0$. For slow $d/dt \ll f, \Omega_i$ motions and with the vanishing of $\nabla p \times \nabla \rho$, the convective structure in fluids and plasmas are quasi-two-dimensional due to this theorem. From the x-y components of Eq. (11) we see that to keep the fluid vorticity $\boldsymbol{\omega}$ pointing in the $\widehat{\mathbf{z}}$ direction in the presence of large $f\widehat{\mathbf{z}}$, the horizontal velocity must satisfy $|\partial_z \mathbf{v}_\perp| \ll f$. The $\widehat{\mathbf{z}}$ component of the vorticity changes according to the vortex stretching given by $\partial_z w - \nabla \cdot \mathbf{v} = -\nabla_\perp \cdot \mathbf{v}_\perp$. The 2D compression occurs from both the change in f given by $\beta = \partial f/\partial y$ and the ageostrophic (polarization) drift velocity.

For $p = p(\rho)$ the vertical ($\widehat{\mathbf{z}}$) component of Eq. (11) reduces to

$$\frac{d}{dt}(f + \omega) = (f + \omega)\frac{\partial w}{\partial z} \tag{12}$$

describing the exponential growth and decay of the absolute vorticity for a given positive or negative value of stretching $\partial w/\partial z$. In the full 3D system we will determine $\partial w/\partial z$ from the total geostrophic convective time derivative of $\partial p/\partial z$ to rewrite Eq. (12) as $dq/dt = 0$. In the 2D limit of shallow water the derivation of $q_G(x, y, t)$ is simple. Integrating Eq. (12) over z from the bottom to the upper free surface and using that at the free surface $w = dH/dt$ gives $H\, d_t(f + \omega) = (f + \omega)(dH/dt)$. Thus $q_G = (f + \omega)/H$ is conserved.

In both the GFD and plasma dynamics of vorticity the finite, or first order, Rossby number R_0 and finite Larmor radius (FLR) effects are essential to determine the horizontal compression $\nabla_\perp \cdot \mathbf{v}_\perp$. Iterating on $1/f$ in the momentum Eq. (9) we obtain the next term in the $1/f$ expansion by evaluating the convective derivative with the geostrophic velocity

$\mathbf{v} = \widehat{\mathbf{z}} \times \nabla p/\rho f$ to obtain the ageostrophic velocity

$$\mathbf{v}_{ag} = -\frac{1}{f}\frac{d}{dt}\left(\frac{1}{f\rho}\nabla_{\perp} p\right). \tag{13}$$

For a single layer of shallow fluid with a free upper surface the height integrated divergence free condition (6) evaluated with ageostrophic flow $\mathbf{v}_{ag} = -(g/f^2)(d\nabla\delta H/dt)$ and the upper boundary condition $w = dH/dt$ yields the reduced form of Ertel's theorem

$$\frac{d}{dt}\left(\frac{f + \frac{g}{f}\nabla^2\delta H}{H_0 + \delta H}\right) = 0 \tag{14}$$

describing the conservation of the potential vorticity $q_{\rm G}$.

For the magnetized plasma the vorticity equation (11) and continuity Eq. (1) yield

$$\frac{d}{dt}\left[\frac{\Omega_i + \frac{c}{B}\nabla^2\Phi}{n(\mathbf{x},t)}\right] = 0 \tag{15}$$

(Meiss and Horton, 1983). Using the Boltzmann relation $n(x,t) = n(x)\exp(e\Phi/T_e(x))$ gives the single PDE for $\Phi(x,y,t)$. The details of this analysis and further comparisons with GFD are given in Horton and Ichikawa (1996, ch. 6).

Comparing Eqs. (14) and (15) we see that for the two analog systems the role of deep water is played by the high plasma density and the gradient of the Coriolis parameter f is equivalent to the gradient of the magnetic field. Both systems have a conserved potential vorticity q with $dq/dt = 0$. The invariants derived from integrals of q, q^2 and the x, y moments of q are key ingredients of the Lyapunov stability analysis of the systems. The Lyapunov stability is treated in Laedke and Spatschek (1986, 1988), Swaters (1986), Sakuma and Ghil (1991), and Nycander (1992), but is too technical to develop here.

Equations (14) and (15) are highly nonlinear and do not have symmetry with respect to the interchange of anticyclonic ($\delta H > 0$ or $\delta\Phi > 0$) and cyclonic ($\delta H < 0$ or $\delta\Phi < 0$) disturbances. Clearly, the anticyclonic (AC) disturbance has $\omega = (g/f)\nabla^2\delta H < 0$ opposite to f so that a localized disturbance may freely drift to larger f or smaller H_0 while conserving

q_H by increasing its strength. The cyclonic (C) disturbance has ω of the same sign as f and may propagate to smaller f while gaining strength.

Reduced dynamical equations showing the broken AC-C symmetry were given in a number of works including Tasso (1967), Petviashvili (1977), Horton and Petviashvili (1993), Nezlin and Snezhkin (1993), and Horton and Ichikawa (1996). Su *et al.* (1991, 1992) investigate the properties of these equations in some detail showing how the Larichev-Reznik (1976) dipoles are split in part with only the anticyclonic vortex forming along lined coherent structure. Nezlin (1994) emphasizes the importance of the anticyclone over the cyclone in Jupiter's atmosphere and other geophysical vortices when the vortex radius r_0 exceeds the Rossby deformation radius ρ_R.

In the local limit where the potential vorticity in Eq. (14) reduces to

$$q_H = \nabla^2 h - \frac{1}{\rho_R^2}\, h + \beta y \tag{16}$$

and in Eq. (15) to

$$q_p = \rho_s^2 \nabla^2 \varphi - \varphi + v_d x \tag{17}$$

the equation $dq/dt = 0$ gives the locally homogeneous pde called the Charney-Hasegawa-Mima equation (hereafter called CHM). The relevant dimensionless coordinates are ρ_R or ρ_s for x, y and the time unit ρ_R/v_R or ρ_s/v_d such that the Rossby/drift speed is unity. In these space-time coordinates the amplitude is scaled as $\rho_R\beta/f \sim \rho_R/R_p \ll 1$ and $\rho_s/L_n \ll 1$ to give the nonlinearity unit strength. Here R_p is the radius of the planet. The CHM equation is then

$$(1 - \nabla^2)\frac{\partial \varphi}{\partial t} + \frac{\partial \varphi}{\partial y} - [\varphi, \nabla^2 \varphi] = 0 \tag{18}$$

where we have taken x in the direction of the inhomogeneity (northward on the planet and radially in the plasma) and y in the symmetry direction.

The nonlinear drift wave equation (18) exhibits both dispersive wave and coherent vortex propagation. The vortex properties dominate, trapping the wake fields, when the amplitude

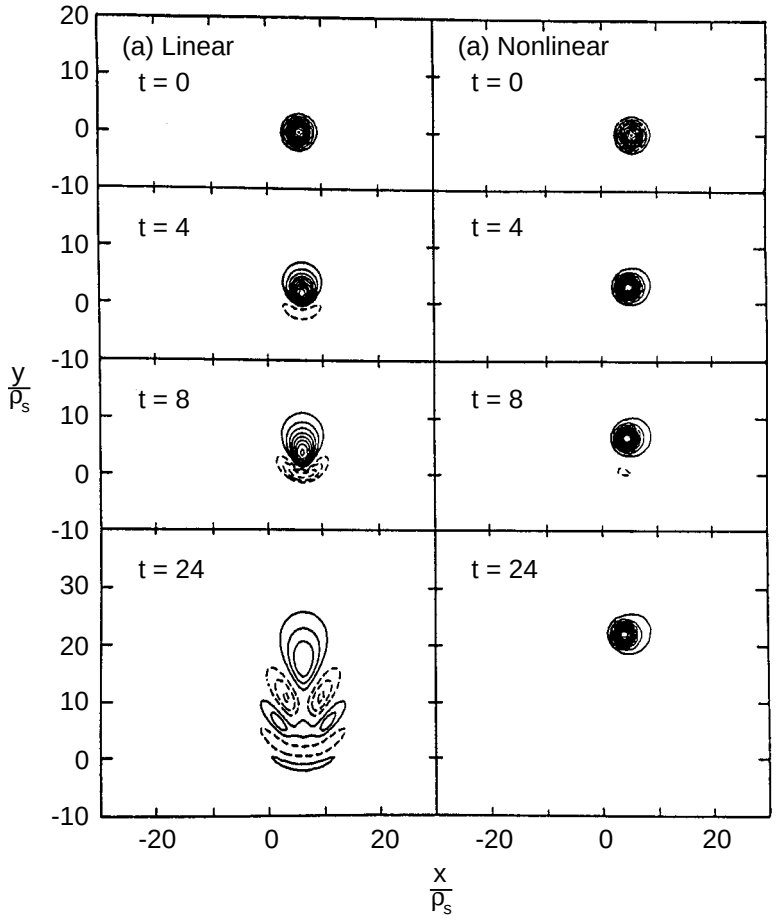

Figure 3: Comparison of the linear and nonlinear drift wave–Rossby wave propagation from an initial gaussian anticyclonic disturbance. The drift wave–Rossby wave speed is unity and in the $\hat{\mathbf{y}}$ direction.

is such that the rotation period in the structure of size $r_0 = \pi/k_\perp$ is shorter than the corressponding wave period $2\pi/\omega_{k_\perp}$. Here r_0 is the radius of the incipient vortex and the trapping condition requires $\max(v_x) = (1/\rho_0 f)(\partial\delta p/\partial y) > v_R$ or $\delta H/H > r_0/R_p$ for the shallow fluid. These properties are illustrated in Fig. 3 which compares the propagation properties of a small amplitude disturbance in the left column with a large amplitude disturbance well above the trapping condition in the right column for an initial gaussian AC distribution. The upward (westward) propagating wave contains wave fronts of speeds from zero to v_R whereas the large amplitude disturbance traps most of the wave energy and propagates coherently at

the speed v_R. The monopolar structure does not have the reflection symmetry required of solution of Eq. (18) $[\varphi(-x, y, t) = -\varphi(x, y, t)]$ so that an underlying odd dipolar component is created in one rotation period. This reflection system is why the exact, localized stationary solutions must have odd mirror or reflection symmetry like the Larichev-Reznik dipolar structures. However, in practice, as Fig. 3b shows that the dominant monopolar structure, with a small dipolar component can form a long-lived, coherent structure. We will see this again in the next example where a monopolar structure is the product of a collision between two dipoles. The wakefield of the linear structure can be computed in detail. The tilted chain of trailing waves is understood from the $\max(\partial\omega/\partial k_x) \cong -2\max(k_x k_y \rho_s^2) v_R$ which occurs for $\theta = \tan^{-1}(k_x/k_y) = 45°$.

In the atmosphere the trapped structure form by either the sudden creation of hot or cold spots by nonadiabatic processes and/or the confluence of counterstreaming flows. Holland (1995) describes both processes operating in the summer Asian monsoons in the western Pacific in the tropics at $\simeq 10°$ N latitude. This region during the summer has a high birthrate of mesoscale vortices, some of which grow into large, long-lived cyclonic depressions. An example at an early state of development given in Fig. 4 from Holland (1995, fig. 15) shows a structure that is similar to the first three vortices shown in the head of the wake in Fig. 3a. Now we consider the interaction and structural stability of the dipolar vortices.

To further illustrate the properties of Eq. (18) let us launch two Larichev-Reznik dipole solutions with opposite polarizations of the electric field or $\nabla\delta H$ — so that they collide. Rather than taking the symmetric co-axial collision, it is more informative to have the dipole centers offset by the impact parameter b comparable to the radius r_0 of the Larichev-Reznik dipoles. The situation is shown in Fig. 5 with $r_0 = 6\rho_R$ and $b = 5\rho_R$. In the coordinates of Eq. (18) the Rossby-drift wave propagates with unit speed in the $+y$ direction (westward). This is also the direction of propagation of the lower dipole in Fig. 5 with the anticyclone on the right and the cyclotron on the left. The upper dipole has the AC on the left and C

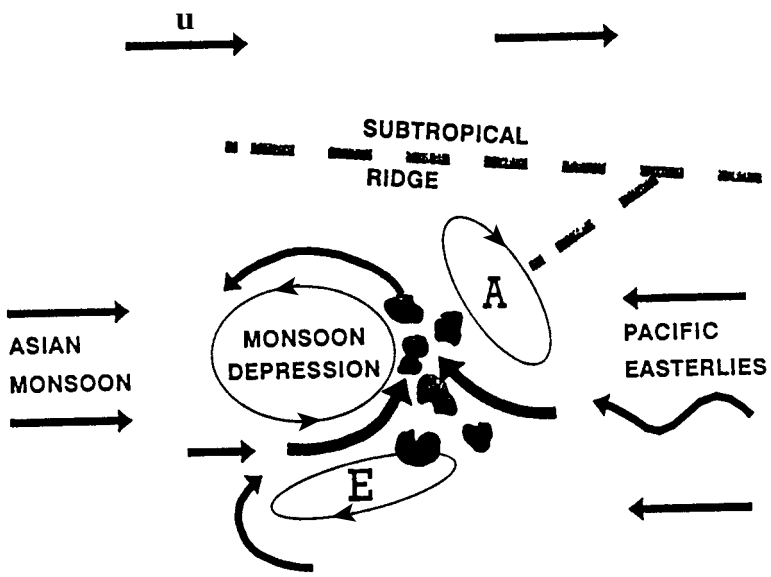

Figure 4: A strong leading cyclonic Rossby wave disturbance with its wakefield of two anticyclonic patches that appears to conform to the wakefield structure shown in Fig. 3a. Other conditions relevant to this southwast Pacific typhoon are given in Holland (1995) (courtesy of Holland).

on the right, and, by itself, will propagate downward (eastward). What we see happening is the merging or coalescence of the two cyclonic regions to form a new, stronger cyclone. The merger is of the type shown in Griffiths and Hopfinger (1986, 1987).

Now, which of the two AC's pair up with the large cyclone depends on the stability of the dipole system with out-of-balance monopolar components. This problem is investigated by Javonović and Horton (1993) using Lyapunov stability theory and simulations. The stability question can be answered, however, using Ertel's theorem with more clarity than using the heavy mathematical machinery of Lyapunov stability theory (Muzylev and Reznik, 1992). First consider the left side AC with the large, central cyclone. The anticlockwise velocity field of the large cyclone rotates the left AC down under itself which strengthens it. The strengthened left AC then rotates the central C to the left, allowing it to strengthen from the reduced f. This result is a stable, oscillatory drift of this C-AC pair while propagating downward (eastward). Now, if one considers the alternative possibility for the central C and

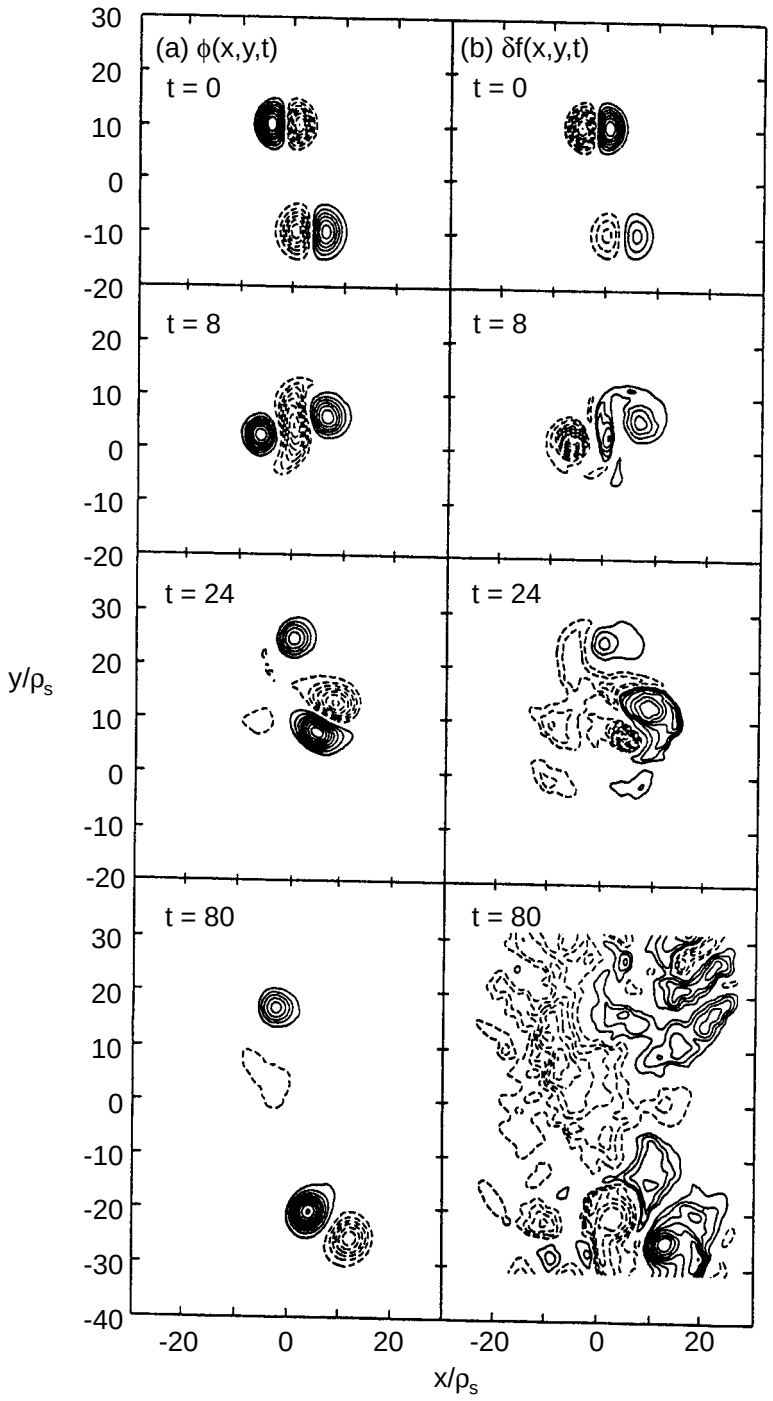

Figure 5: Collision of opposite polarity drift wave vortices with impact parameter $b = 5\rho_s$ and dipole radius $a = 6\rho_s$. (a) 15 contours of potential with the range ± 54.7 at $t = 0$ and -49.5 to 65.5 at $t = 80$; (b) 15 contours for perturbed distribution δf with the range ± 54.7 at $t = 0$ and -10.4 to 13.3 at $t = 80$. Positive values of the functions are solid lines and negative values are dashed.

the right hand AC joining together, the system falls apart. The right side AC is weakened by its rotation from the large cyclone. Thus, they (the C and right-hand AC) do not bind. In fact, the same arguments are easy to use to show why the westward propagating dipole is unstable to a slight de-symmetrization of the dipole lobe strengthens. The motion is such that the initially stronger lobe continues to gain strength by drifting farther to the north (for the $AC > C$) or to the south (for the $C > AC$).

This is in accordance with the mathematical stability analysis (Laedke and Spatschek, 1988) indicating that the eastward (ion-diamagnetic direction) dipole is stable. Difficulties in giving a complete mathematical proof of stability are described by Nycander (1992). The simulations and the point vortex models (Kono and Horton, 1991) and Hobson (1991) give clear physical pictures for why the westward dipole is unstable. These stability properties may account for the rather uncommon occurrence of the dipole structures in the atmosphere. The effect of the temperature gradient is another reason for the lack of the dipoles (Jovanović and Horton, 1993).

The collision is also inelastic with a wakefield generated similar to that shown in Fig. 3. The right-hand side of Fig. 5 shows the contours of a passive field f convected by the flow. The initial value of the passive f is trapped inside the dipoles.

1.3 Vertical motion in the stably stratified medium

The stable vertical stratification of the fluid introduces the restoring force from the buoyancy of the fluid. This buoyancy frequency

$$N = (-g\partial_z \ell n\, \rho)^{1/2} \tag{19}$$

follows from the convection of the density perturbation $\delta\rho$ by the vertical velocity w

$$\frac{d\delta\rho}{dt} + w\,\frac{\partial\rho_0}{\partial z} = 0 \tag{20}$$

and the vertical acceleration

$$\rho_0 \frac{dw}{dt} = -\frac{\partial}{\partial z}\,\delta p - g\delta\rho. \tag{21}$$

Here d/dt is the horizontal convective derivative with the geostrophic velocity. Taking d/dt of Eq. (21) and using Eq. (20) for $d\delta\rho/dt$ gives

$$\frac{d^2}{dt^2}\,w = -N^2 w - \frac{d}{dt}\left(\frac{1}{\rho}\,\frac{\partial}{\partial z}\,\delta p\right). \tag{22}$$

Thus, perturbed vertical pressure gradients drive vertical oscillations at the frequency N about the initial stratified equilibrium position. For motions on long-time scales $\Delta t \gg 1/N$ compared to the rapid (small amplitude) vertical motion, the time-averaged vertical velocity is

$$w = \frac{-1}{N^2}\,\frac{d}{dt}\left(\frac{1}{\rho}\,\frac{\partial \delta p}{\partial z}\right), \tag{23}$$

following from the time-average of Eq. (22).

This determination of w is the primary difference with the plasma confinement where the equilibrium is uniform along $\mathbf{\Omega} = \Omega\hat{\mathbf{z}}$ with neutral stability with respect to translations along $\hat{\mathbf{z}}$. There are stable oscillations along $\hat{\mathbf{z}}$ in the plasma, but they are associated with the ion-acoustic waves $k_\parallel^2 c_s^2$ with $c_s^2 = T_e/m_i$ not with stratification or an equilibrium restoring force. The acoustic waves are low in frequency compared with $\Omega_i = eB/m_i c$. The acoustic waves occur both above and below the drift wave frequency depending on the ratio of $k_\parallel c_s/k_y v_{de} = k_\parallel L_n/k_y\rho_s$.

Equation (23) describes the vertical outflow from a growing, localized high pressure (AC) region. There is a balancing inward horizontal flow from the ageostrophic velocity. Balancing the divergence of the inward horizontal flow with the outward vertical flows gives the basic quasigeostrophic baroclinic equation for the eigenmodes of the system. Substituting Eq. (23) into Eq. (12) gives

$$\frac{d}{dt}\left\{f(y) + \frac{1}{f\rho_0}\,\nabla_\perp^2 \delta p + \frac{\partial}{\partial z}\,\frac{f}{N^2\rho_0}\,\frac{\partial \delta p}{\partial z}\right\} = 0 \tag{24}$$

where $df/dt = (\beta/f\rho_0)\partial_x \delta p$. The vertical eigenmodes with $w = 0$ at $z = 0$ and $z = D$ are approximately $\delta p_n = \delta p_n(x, y, t)\cos(n\pi z/D)$ giving the horizontal dynamics

$$\frac{d}{dt}\left[\frac{1}{\rho_0}\nabla_\perp^2 \delta p_n - \frac{f^2}{N^2 D_n^2}\,\delta p_n\right] + \frac{\beta}{\rho_0}\frac{\partial}{\partial x}\,\delta p_n(x, y, t) = 0. \tag{25}$$

For a sufficiently smooth $N(z)$-profile the eigenvalues are $D_n = D/n\pi$. For a strongly localized $N(z)$ of height Δz_m there are trapped internal modes when $k_\perp N_{\max}\Delta z_m > \pi f$ where $k_\perp = (k_x^2 + k_y^2)^{1/2}$ is the horizontal wavenumber.

Thus, the internal Rossby deformation radius ρ_R is

$$\rho_R(n) = ND_n/f \tag{26}$$

where $\rho_R(n = 0) \to \infty$ for the barotropic (flute) mode and $\rho_R(n = 1) \simeq ND/\pi f$ for the first baroclinic mode. The relation with the shallow water Rossby radius is found by noting that $N = [(\Delta\rho/\rho)(g/D)]^{1/2}$ so that $\rho_R(n = 1) \to [Dg(\Delta\rho/\rho)]^{1/2}/f < (gH)^{1/2}/f$. For the oceans the effect of $\Delta\rho/\rho$ and the eigenmode calculation is to lower $\rho_R(n = 1)$ to about 80 km. Thus, the oceans have a much smaller value of $\rho_R/R_p \sim 10^{-2}$ more analogous to the magnetic confinement experiments. Another, unfortunate, analogy of the oceans with the plasmas is that detecting the Rossby wave structures in the oceans is much more difficult than in the atmosphere.

2 Horizontal Temperature Gradients

Both magnetized plasmas and geophysical fluids are subjected to localized heating and cooling resulting in substantial temperature gradients. The resulting temperature gradients can drive large-scale convective motions that serve to transport thermal energy and momentum. The stability analysis of the various equilibrium models is a classical problem in both fields. Here we briefly compare the systems before showing the results for the plasma simulations.

The linear stability analysis gives an expression for the growth rate $\gamma^\ell(\mathbf{k}, \{\mu\})$ for the mode as a function of wave vector $\mathbf{k}$ and the system parameters $\{\mu\}$. Generally, the fluctu-

ations that maximize $\gamma_{\mathbf{k}}^{\ell}$ provide the dominant source of energy into the convection system. The temperature gradient modes have a well-defined maximum growth rate at the wavenumber $k_{\perp} \sim \rho^{-1}$ where $\rho = \rho_I = ND/f$ in the baroclinic instability and $\rho = \rho_s = (m_i T_e)^{1/2}/eB$ in the magnetized plasma.

2.1 Baroclinic instability

The baroclinic instability mechanism is a modification of the Rayleigh-Benard instability taking into account the role of the Coriolis force in the momentum equation and the constraints of the vertical stratification. The thermal energy release is driven by the gravitational potential energy obtained by interchanging lighter and heavier fluid parcels taking into account their change in density $\rho = \rho(p, T)$ with temperature and pressure. For liquids the equation of state is simpler with $\rho = \rho(T)$ for the usual range of pressures.

For the oceans and the rotating water tanks (liquids) the fractional change in density is very small with $\rho = \rho_0(1 - \alpha(T - T_0))$ with $\alpha = 2 \times 10^{-3}/^{\circ}C$ for water. Thus the Boussinesq approximation applies where $\rho = \rho_0 =$ const except in the buoyancy term where $g\delta\rho = -g\rho_0\alpha\delta T$. Gravitational potential energy is released to drive convection when the lower level fluid is heated becoming lighter or the upper level is cooled becoming heavier.

For the atmosphere and plasma (gases) the compressibility of the gas determined by the ratio of the specific heats $\Gamma = C_p/C_v$ must be taken into account. For the diatomic atmosphere gases $\Gamma = 1.4$ while for the collisionless plasma the value of Γ ranges from 5/3 to 3 as the effective number of degrees of freedom involved in the dynamics changes from three to one. For the ITG instability the effective Γ is given in Kim and Horton (1991) from kinetic theory considerations. For the ideal gas equation of state $\rho = P/nRT$ so that the volume expansion coefficient $\alpha = -\partial \ell n\, \rho/\partial T)_p = 1/T \sim 3 \times 10^{-3}/^{\circ}C$ at $T \sim 300^{\circ}$ K.

In the geophysical problem the effect of the horizontal temperature instability is complicated by the vertical stratification of the fluid described in Sec. 1.3. For instability the

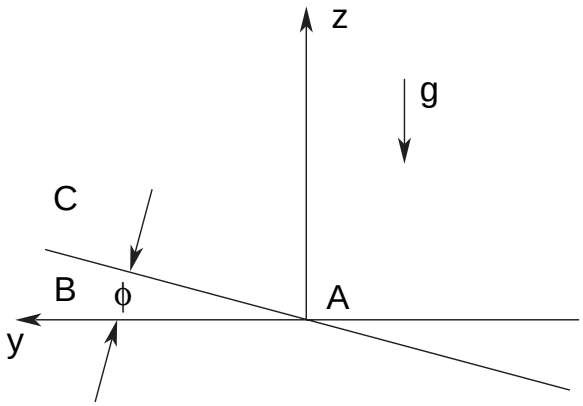

Figure 6: For the sloping constant density surfaces at angle ϕ from the horizontal, gravitational potential energy is released by the interchange of fluid elements between A and B.

buoyancy must be overcome by suitable restrictions on $\mathbf{k}, \omega$ in geostrophic motions to give rise to growth of the convection. To understand the origin of these restrictions consider the sloping contours of the potential temperature and density shown in Fig. 6. Both Pedlosky (1987, p. 519) and Gill (1982, p. 555) begin their discussion of the baroclinic instability by calculating the gravitational potential energy released resulting from interchange motions for the sloping contours shown in Fig. 6. The angle ϕ (in radians) of the slope of the isotherms and isopycnals (constant density surfaces) required for fast-growing modes is very small. It is evident (see Pedlosky and Gill for the calculation) that only interchanges of fluid parcels A and B, within the small wedge of angle ϕ, will release potential energy. Interchange of A and C requires work be down against g due to the stable stratification.

In the toroidal plasma confinement device the equilibrium pressure, density and temperature are independent of z having gradients perpendicular to $\mathbf{B}$. The role of gravity g is played by the curvature and gradient-B drifts of the charged particles producing through charge separation an effective gravity term from the electric acceleration acting across the magnetic field $\mathbf{\Omega}_i$. The electric field produces an interchange of plasma that is mathematically of the same form as that with the gravitational acceleration component $\mathbf{k} \cdot \mathbf{g} \times \nabla \rho = k_x g \, \partial \rho / \partial y$ of

the neutral fluid. The interchange is effective in lowering the plasma thermal energy. The effective plasma g is given by $g = c_s^2/R_c$ where R_c is the radius of curvature of the field lines (Hazeltine and Meiss, 1992).

To understand the conditions on the $\mathbf{k}, \omega$ for the release of potential energy we analyze the temperature equation $dT/dt = 0$ for the incompressible liquid or the adiabatic equation $d\theta/dt = 0$ for the compressible gas or plasma. Here $\theta = \theta_0(p/p_0)^{1/\Gamma}(n_0/n)$ is the potential temperature and $\Gamma = C_p/C_v$ the ratio of specific heats.

For liquids with $\Delta\rho/\rho = \alpha\Delta T < 10^{-2}$ the Boussinesq approximation is valid. In the Boussinesq equations $\rho = \rho_0 =$ constant everywhere except in the buoyancy term where

$$\delta\rho g = -\alpha\rho_0\delta T = -\partial(\delta p)/\partial z \tag{27}$$

for slow motions that avoid the stabilizing vertical oscillations.

For the atmosphere the compression due to Γ is retained by working with $\theta = \theta_0 + \delta\theta$ where $\delta\theta/\theta_0 = -\delta\rho/\rho_0 + \delta p/\Gamma p_0$ for adiabatic motion. Pedlosky (1987, p. 365) introduces the horizontal velocity streamfunction $\psi = \delta p/f\rho_0$ and uses $g\delta\rho = -\partial_z\delta p$ to show that

$$\left(\frac{g}{f}\right)\frac{\delta\theta_0}{\theta_0} = \partial_z\left(\frac{\delta p}{f\rho_0}\right) \tag{28}$$

when $\partial z \ell n\, \rho_0 = -g/c^2$ with $c^2 = \Gamma p_0/\rho_0$.

The equilibrium constant-slope surfaces of Fig. 6 are given by $\theta = \theta_0(z - \phi y)$ and $\rho = \rho_0(z - \phi y)$. The perturbation in the temperature δT, or perturbed potential temperature $\delta\theta$, in the absence of thermal diffusion $\omega \gg k^2\chi$ is governed by

$$\left(\frac{\partial}{\partial t} + u\,\frac{\partial}{\partial x}\right)\delta\theta + (-v\phi + w)\,\frac{\partial\theta_0}{\partial z} = 0 \tag{29}$$

where we use $\partial\theta_0/\partial y = -\phi\partial\theta_0/\partial z$ due to the slope ϕ. Multiplying Eq. (29) by g/θ_0 and recognizing that the Brunt-Väisälä buoyancy frequency is

$$N^2 = \frac{g}{\theta_0}\,\frac{\partial\theta_0}{\partial z} \tag{30}$$

and using Eq. (28) we obtain

$$-i(\omega - k_x u)\frac{\partial}{\partial z}\left(\frac{\delta p}{\rho_0}\right) + N^2(-\phi v + w) = 0. \tag{31}$$

From Eq. (31) it is clear that the stable vertical oscillations from the buoyancy restoring effect $N^2 w$ in Eq. (31) are lost when

$$w(-\phi v + w) < 0. \tag{32}$$

A simple estimate of the conditions on $\mathbf{k}, \omega$ implied by condition Eq. (32) is obtained from the shallow water equations $w = d\delta H/\delta t = -i\omega\delta H$ and $v = (g/f)\partial_x \delta H = i(k_x g/f)\delta H$ giving the necessary condition

$$\omega(\omega - \omega_*) < 0. \tag{33}$$

for instability where $\omega_* = -k_x g\phi/f$. A sufficient condition for instability requires finding the actual dynamics required to release the energy by solving for the wave function and eigenvalues as in the Eady problem, for example. The shallow water approximation shows that for $\phi \sim 10^{-4}$ and $k_x \sim 10^{-4} m^{-1}$ waves with $\omega \lesssim 10^{-4}\, s^{-1}\,\mathrm{Hz}$ satisfy $\omega < \omega_*$. The phase velocity ω/k_x must be parallel to $\nabla\rho \times \mathbf{g}$ and low enough to release the potential energy ($\phi v > w$). Without the $\beta = \partial f/\partial y$ effect the $\widehat{\mathbf{y}}$-direction is the direction of the local temperature gradient without regard to the north-south direction. An estimate for ω_* taking into account the 3D nature of the baroclinic motion is obtained by using w from Eq. (23) and $v = ik_x \delta p/\rho_0 f$ in Eq. (31). The result is $\omega_*(3D) = k_x\, DN^2\phi/f$ whereupon using $\rho_I = ND/f$ gives

$$\omega_* \cong k_x \rho_R\, N\phi. \tag{34}$$

Thus, for $k_x\rho_R \sim 1$ the upper limit of ω_* and the growth rate γ of the unstable mode is $N\phi$. For large slopes $\phi \sim f/N \sim 10^{-2}$ the instability breaks the quasigeostrophic condition $|\omega| \ll f$. This regime may occur in sharp fronts.

The classical baroclinic instability analysis (the Eady and Charney problems, Gill, 1982, pp. 556–563) is briefly given for completeness. The linearization of Eq. (24) gives vertical eigenvalue problem

$$\left[\frac{d^2}{dz^2} - \frac{N^2 k_\perp^2}{f^2}\left(1 + \frac{k_x \beta}{\omega k_\perp^2}\right)\right]\frac{\delta p}{\rho_0} = 0 \tag{35}$$

with solutions

$$\frac{\delta p}{\rho_0} = A\sinh(qz) + B\cosh(qz) \tag{36}$$

where $q = (k_\perp N/f)(1 + k_x\beta/\omega k_\perp^2)^{1/2}$. Equation (31) determines $w_k(z)$ since all other terms are known from Eq. (36) with $v = (ik_x/f)(\delta p/\rho_0)$. Now the vertical equilibrium $g\rho(z - \phi y) = -\partial p/\partial z$ demands that there is shear in the horizontal velocity $u(z) = -(1/\rho_0 f)\partial p/\partial y$ with $\partial u/\partial z = \phi N^2/f$.

The simplest case is the Eady problem which has a rigid lid so that $w = 0$ at both $z = \pm D/2$ and has $\beta = 0$. The eigenvalues follow from substituting Eq. (36) into Eq. (31) and evaluating the equation at $z = \pm D/2$. The determinant of the 2×2 system in the A, B coefficients yields

$$\omega = \pm i\,\frac{|k_x|\phi N^2 D}{f}\left[\left(\coth\left(\frac{qD}{2}\right) - \frac{qD}{2}\right)\left(\frac{qD}{2} - \tanh\left(\frac{qD}{2}\right)\right)\right]^{1/2} \tag{37}$$

for the unstable complex conjugate modes for $qD < 2.4$. The modes (37) coalesce and go to stable modes for $qD = k_\perp N D/f > 2.4$. The maximum growth rate $\gamma_{\max} = 0.31 f u'/N = 0.31 N\phi$ occurs at $k_y \to 0$ and $k_x(ND/f) = 1.6$ corresponding to a wavelength $2\pi/k_x \simeq 4\rho_I = 4(ND/f)$. Pedlosky states that for $\rho_I \cong 10^3$ km this wavelength is in excellent agreement with the most energetic synoptic scale atmospheric disturbances. Monin (1972) shows the energy spectrum in Fig. 7 computed from wind fluctuations with a pronounced peak at a period corresponding to approximately 100 hr $\sim$ 4 days that agrees with the baroclinic instability as the source of energy into the spectrum. The wavelength corresponding to the peak is approximately such that $k_x \simeq m/R_0$ with $m \cong 6$ consistent with $\lambda \sim 4000$ km and $R_0 = R_E \cos\theta \approx 4000$ km at $\theta = 30°$.

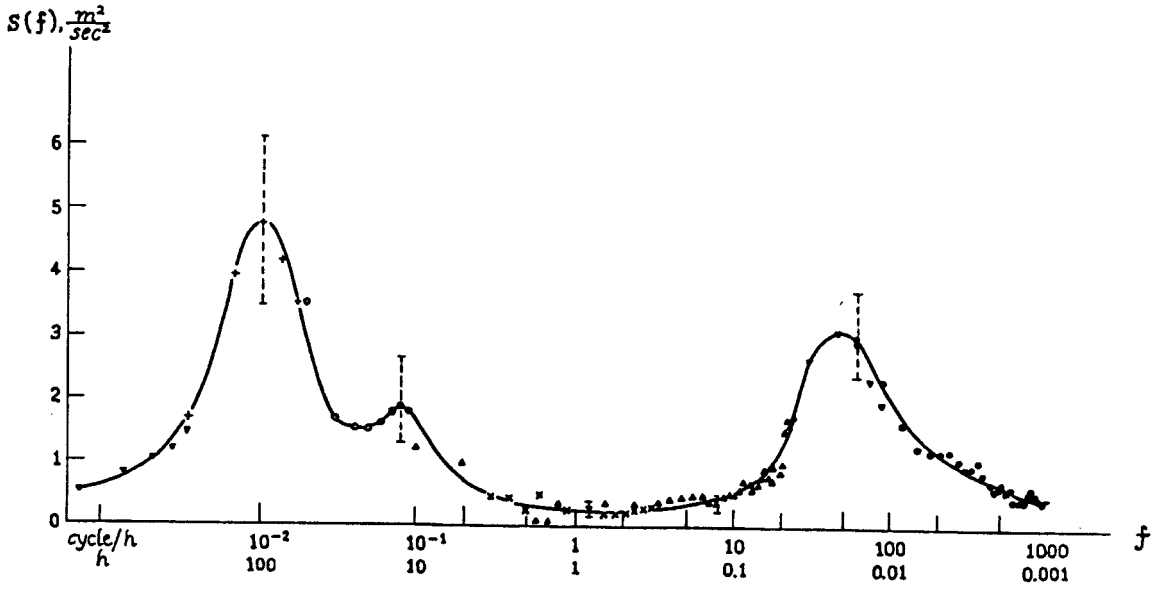

Figure 7: Energy-like spectrum $fS(f)$ constructed from the power spectrum $S(f)$ of the horizontal wind velocity time series taken from Monin (1972). The dominant peak in the spectrum is at a period of $100\,h \approx 4$ days. Monin interprets the peak as the position of the energy injection from the large baroclinic instability. For $\rho_R = 10^3$ km the peak corresponds to $k_x \rho_R = 1$ for a longitudinal mode number $m = 6$ (from Monin, 1972).

The situation for tokamaks is that with substantial ion heating a peak in the fluctuation spectrum appears at $k_\perp \rho_s \sim 0.5$ that is identified (Brower *et al.*, 1987, 1989) with the ion temperature gradient by the direction of propagation being in the direction parallel to $\mathbf{B} \times \nabla p_i$ (corresponding to eastward in the Rossby Wave–Drift Wave analog). The electron drift wave spectrum (westward Rossby wave) is universally present: whereas the ion feature in the spectrum occurs only when the ion temperature gradient exceeds the adiabatic gas threshold condition.

2.2 Nonlinear dynamical equations for the Baroclinic instability

For the case of a liquid the equation of state is simpler than for a gas or plasma with the standard model taking the linear relation $\rho = \rho(T) = \rho_0 [1 - \alpha(T - T_0)]$. In this case $d\rho/dt = \rho' dT/dt = \rho' \chi \nabla^2 T$ where χ is the thermal diffusivity. In this model the fluctuation

dynamics for fixed $\partial\rho/\partial y \propto \partial T/\partial y$ suitable for numerical integration are given by

$$\frac{d}{dt}\left(\frac{\nabla_\perp^2 \delta p}{f\rho_0}\right) + \frac{\beta}{f\rho_0}\frac{\partial}{\partial x}\delta p = f\frac{\partial w}{\partial z} + \frac{\mu}{f\rho_0}\nabla_\perp^4 \delta p \tag{38}$$

$$\rho_0 \frac{dw}{dt} = -g\delta\rho - \frac{\partial}{\partial z}\delta p \tag{39}$$

$$\frac{d}{dt}\delta\rho + \frac{1}{f\rho_0}\frac{\partial\rho_0}{\partial y}\frac{\partial}{\partial x}\delta p + \frac{\partial\rho_0}{\partial z}w = \chi\nabla^2\delta\rho. \tag{40}$$

For the liquid we may take $\rho_0, \partial\rho_0/\partial y$ and $\partial\rho_0/\partial z$ constant throughout the volume Ω of the system which simplifies the analysis and simulations. Equation (38) is the same vorticity equation as in the Rossby waves, but now the vortex stretching by the vertical velocity w is controlled by the change in $\delta\rho$ both through horizontal convection and vertical convection.

The stable vertical stratification is overcome and the total fluctuation energy grows exponentially due to the horizontal temperature gradient $\partial T/\partial y = (-1/\alpha\rho_0)(\partial\rho_0/\partial y)$. In the steady state the energy production by the meridional thermal flux balances the dissipation in Eqs. (38)–(40). To demonstrate this balance we need to analyze the flow of fluctuation energy through the system (38)–(40). Multiply Eq. (38) by $\delta p/f_0$, Eq. (39) by w and Eq. (40) by $\delta\rho$ and integrating over the volume Ω yields

$$\frac{\partial}{\partial t}\left[\frac{1}{2}\int\limits_\Omega \frac{(\nabla_\perp\delta p)^2}{f^2\rho_0}\,d^3x\right] = -\int\limits_\Omega \delta p\frac{\partial w}{\partial z}\,d^3x - \frac{\mu}{f^2\rho_0}\int\limits_\Omega (\nabla_\perp^2\delta p)^2 d^3x \tag{41}$$

$$\frac{\partial}{\partial t}\left[\frac{1}{2}\int\limits_\Omega \rho_0 w^2\,d^3x\right] = -g\int\limits_\Omega w\delta\rho\,d^3x - \int\limits_\Omega w\frac{\partial\delta p}{dz}d^3x \tag{42}$$

$$\frac{\partial}{\partial t}\left[\frac{1}{2}\int\limits_\Omega \delta\rho^2 d^3x\right] = -\frac{\partial\rho_0}{\partial z}\int\limits_\Omega \delta\rho w d^3x - \frac{\partial\rho_0}{\partial y}\int\limits_\Omega \delta\rho v d^3x - \chi\int\limits_\Omega (\nabla\delta\rho)^2 d^3x. \tag{43}$$

For simplicity the boundary surface integrals over $\partial\Omega$ have been dropped. Thus the three fluxes $\langle\delta p\,\partial w/\partial z\rangle$, $\langle w\delta p\rangle$ and $\langle\delta\rho\,v\rangle$ transfer energy between the kinetic and potential energy components

$$K_\perp = \frac{1}{2}\int\limits_\Omega \rho_0(u^2+v^2)d^3x, \tag{44}$$

$$K_z = \frac{1}{2}\int\limits_\Omega \rho_0 w^2 d^3x. \tag{45}$$

and

$$U = g\int\limits_\Omega z\rho d^3x = \left[\frac{-g}{(\partial\rho_0/\partial z)}\right]\frac{1}{2}\int\limits_\Omega \delta\rho^2 d^3x \tag{46}$$

is the potential energy. To show the last relationship for the potential energy one uses that for $d\rho/dt = 0$ the Casimir $\int\limits_\Omega \rho^2 d^3x = \int\limits_\Omega (\rho_0 + z\rho_0' + \delta\rho)^2 d^3x$ is a constant of the motion.

Combining Eqs. (40)–(43) yields

$$\frac{d}{dt}\int\limits_\Omega \left[\frac{\rho_0}{2}(\nabla_\perp\psi)^2 + \frac{\rho_0}{2}\,w^2 - \frac{g}{\partial\rho_0/\partial z}\,\frac{(\delta\rho)^2}{2}\right] d^3x \tag{47}$$

$$= g\phi\int\limits_\Omega v\delta\rho d^3x - \mu\rho_0\int\limits_\Omega (\nabla^2\psi)^2 d^3x + \frac{g\chi}{\partial\rho_0/\partial z}\int\limits_\Omega (\nabla\delta\rho)^2 d^3x. \tag{48}$$

From the first energy integral we see that the requirement of stable vertical stratification leads to the positive definiteness of the energy integral W. For stable stratification the system has a linear instability driven by the slope $\phi = -(\partial\rho_0/\partial y)/(\partial\rho_0/\partial z)$. In the nonlinear steady saturated state of this instability Eq. (48) states that the product of the thermal flux proportional to $\phi\int v\delta\rho d^3x$ which multiplied by g balances the dissipation due to small scale viscosity μ and thermal diffusivity χ to produce the saturated state.

In the form given here with *three* pdes in Eqs. (38)–(40) the baroclinic instability dynamics is similar in form to the ITG plasma equations. This is not the case when the further reduction to the quasi-geostrophic form is made as follows. For the stably stratified medium the vertical velocity w adjusts adiabatically to $\partial_z\partial p$ such that Eq. (23) for w applies. Then $\delta\rho = -g^{-1}\partial_z\delta p$ and the energy integral w now reduces to $W \to W_g$ with

$$W_g = \int\limits_\Omega \left[\frac{\rho_0}{2}(\nabla_\perp\psi)^2 + \frac{\rho_0 f^2}{2N^2}(\partial_z\psi)^2\right] d^3x \tag{49}$$

which is the energy associated with gyrostrophic motions. The minimization of W with respect to ψ gives the elliptic baroclinic ($\beta = 0$) equation for $\psi(x, y, z)$.

2.3 Temperature gradient driven convection in magnetized plasma

The plasma equations for temperature gradient driven convection have $f \to \Omega_i (\sim 10^8/\mathrm{s})$, $\rho_R \to \rho_s (\sim 0.1\,\mathrm{cm})$ and $\varepsilon = \rho_s/L_n \sim 0.1\,\mathrm{cm}/10\,\mathrm{cm} = 10^{-2}$. The growing linear modes occur for $k_\parallel L_n < k_y \rho_s < 1$ with $k_y^{\max} \sim 1/2\rho_s \sim 5\,\mathrm{cm}^{-1}$ and $\gamma^{\max} \sim 0.1 c_s/L_T \sim 10^5/\mathrm{s}$ being typical. The signature of the ITG mode in the laboratory plasma is propagation of part of the drift wave fluctuation spectrum in the ion diamagnetic direction ($\sim$ eastward). This is opposed to the resistivity and electron-wave Landau resonance instability that occurs for the usual universal drift wave fluctuations propagating in the electron diamagnetic direction ($\sim$ westward). For example, in the Ohmically heated TEXT tokamaks ($R/a = 1\,\mathrm{m}/0.27\,\mathrm{m}, B = 2\,\mathrm{T}, I = 0.3\,\mathrm{MA}$ the electron drift wave fluctuations are always present, but the fluctuations characteristic of the ion temperature gradient only appear when the conditions are such as to have $\eta_i = d\ell n\, T_i/d\ell n = L_n/L_{T_i} > 1$ and $T_i \simeq T_e$.

With powerful auxiliary heating in the large fusion devices ($I > 1\,\mathrm{MA}$), conditions with $T_i/T_e > 3$ and $\eta_i \gg 1$ are achieved and the signatures of the ion temperature gradient driven turbulence are widely reported. In these devices the power balance analysis reveals that the effective ion thermal diffusivity $\chi_i > \chi_e$ and χ_i values consistent with the ∇T_i-driven drift waves. The value of χ_i inferred from power balance is typically consistent with the mixing length estimate $\chi_i = \gamma^{\max}/k_\perp^2 = (10^5/\mathrm{s})/(5\,\mathrm{cm}^{-1})^2 = 5 \times 10^3\,\mathrm{cm}^2/\mathrm{s} = 0.5\mathrm{m}^2/\mathrm{s}$. The ratio of this turbulent χ_i to the collisional (neoclassical) χ_i^{neo} varies widely from machine to machine and over the radius of a given discharge but is substantially greater than unity (Scott *et al.*, 1994). A detailed stability-transport analysis of a key ITG experiment in the TFTR tokamak may be found in the team project Horton *et al.* (1992). A critique of ITG theory is found in Ottaviani *et al.* (1997).

Here we briefly describe the ITG dynamics indicating some similarities and differences with the baroclinic instability. The vorticity equation arises from the condition $\nabla \cdot \mathbf{j} = 0$

stating that current loops must be closed in the quasineutral plasma. The large $\mathbf{v}_E = c\mathbf{E}\times\mathbf{B}/B^2 = c\widehat{\mathbf{z}}\times\nabla\Phi/B$ velocities cancel in the current $\mathbf{j}$ so that the ion current from the finite inertia (polarization) drift $\mathbf{v}_p$, corresponding to the ageostrophic drift,

$$\mathbf{v}_p = \frac{-c^2 m_i}{eB^2}\left(\frac{\partial}{\partial t} + (\mathbf{v}_E + \mathbf{v}_D)\cdot\boldsymbol{\nabla}\right)\boldsymbol{\nabla}_\perp\Phi, \tag{50}$$

balances the divergence of the parallel current $\nabla_\parallel j_\parallel$. Since the ion fluid is hot $T_i/T_e \gtrsim 1$ the ion gyroradius $\rho_i = c(m_i T_i)^{1/2}/eB \gtrsim \rho_s$ and there are important collisionless stresses from $\nabla\cdot\boldsymbol{\pi}_i(\mathbf{v}_E)$ — the divergence of the off-diagonal terms in the momentum stress tensor $m_i n_i \langle v_\alpha v_\beta\rangle = p_i\delta_{\alpha\beta} + \pi_{i,\alpha\beta}$ where $\pi_{i,\alpha\beta}$ is a linear function of $\partial v_E/\partial x$. The effect of the stress tensor shows up as the new term $K\nabla_\perp^2\partial_y\phi$ in the vorticity equation giving the change of the drift wave propagation at short wavelengths to the ion diamagnetic direction. In Fig. 8 we show the result of repeating the initial value experiment given in Fig. 3 for the ITG equations. Now we see that the long wavelength waves propagate in the electron direction (upward) while the short wavelength modes propagate in the ion diamagnetic direction (downward). The right panel shows that the nonlinear binding effect still applies to the ITG mode fluctuations.

The appropriate dimensionless space-time variables are

$$\widetilde{x} = \frac{x - x_0}{\rho_s}, \quad \widetilde{y} = \frac{y}{\rho_s}, \quad \widetilde{z} = \frac{z}{L_n}, \quad \tau = \frac{tc_s}{L_n}. \tag{51}$$

and the amplitudes of the fluctuations scale as

$$\phi = \left(\frac{e\widetilde{\Phi}}{T_e}\right)\left(\frac{L_n}{\rho_s}\right),$$

$$v = \left(\frac{\widetilde{v}_\parallel}{c_s}\right)\left(\frac{L_n}{\rho_s}\right), \tag{52}$$

$$p = \left(\frac{\widetilde{p}_i}{p_{i0}}\right)\left(\frac{L_n}{\rho_s}\right)\left(\frac{T_i}{T_e}\right). \tag{53}$$

The $\mathbf{E}\times\mathbf{B}$ convective derivative is

$$\{f,g\} = \widehat{\mathbf{z}}\cdot\nabla_\perp f\times\boldsymbol{\nabla}_\perp g = \frac{\partial f}{\partial\widetilde{x}}\frac{\partial g}{\partial\widetilde{y}} - \frac{\partial f}{\partial\widetilde{y}}\frac{\partial g}{\partial\widetilde{x}}, \tag{54}$$

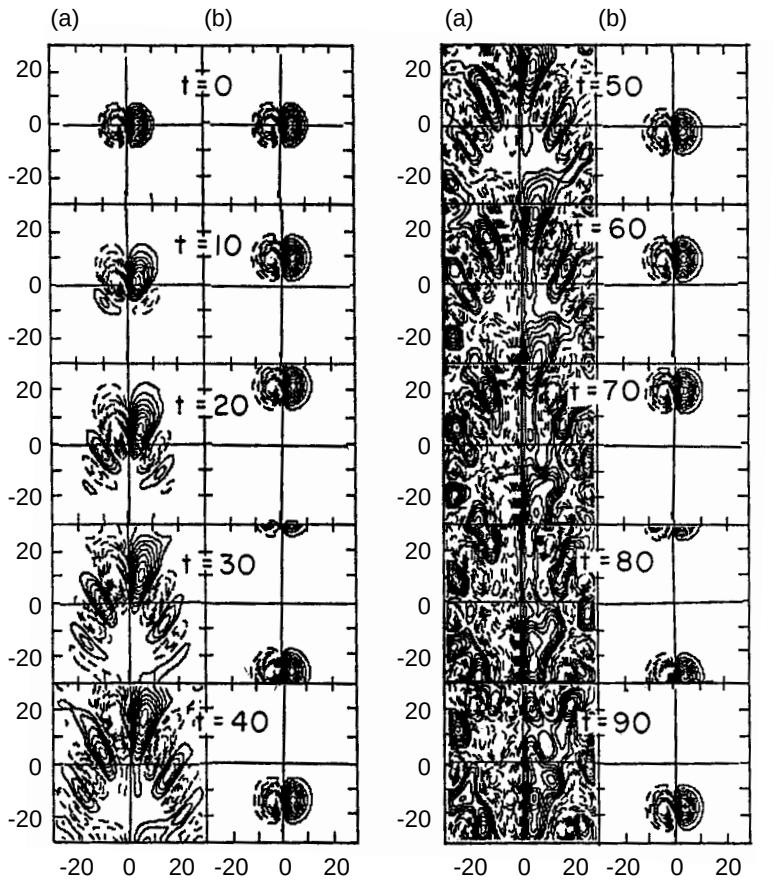

Figure 8: Same as Fig. 3 but for the ion temperature gradient vorticity equation. Now the long wavelength components propagate upward (westward) and the short wavelength components propagate downward (eastward). The strong nonlinear self-binding is still a dominant effect.

and due to the shearing of the helical magnetic field

$$\mathbf{B} = B\left\{\widehat{\mathbf{z}} + \left[\frac{(x-x_0)}{L_s}\right]\widehat{\mathbf{y}}\right\}, \tag{55}$$

the parallel derivative $\mathbf{B}\cdot\boldsymbol{\nabla} = B\nabla_\parallel$ is given by

$$\boldsymbol{\nabla}_\parallel = \frac{\partial}{\partial\widetilde{z}} + S\widetilde{x}\,\frac{\partial}{\partial\widetilde{y}} \tag{56}$$

where $S = L_n/L_s$ measures the strengths of the magnetic shear. (Note that $S = 0$ is a well-defined limit applicable to cylindrical devices.)

The ITG convective turbulence is then described by

$$(1-\nabla_\perp^2)\frac{\partial\phi}{\partial\tau} = -(1+K\nabla_\perp^2)\frac{\partial\phi}{\partial\widehat{y}} - \boldsymbol{\nabla}_\parallel v + \{\phi,\nabla_\perp^2\phi\} - \mu_\perp\nabla^4\phi, \tag{57}$$

$$\frac{\partial v}{\partial\tau} = -\boldsymbol{\nabla}_\parallel(\phi+p) - \{\phi,v\} + \mu_\perp\nabla_\perp^2 v + \mu_\parallel\nabla_\parallel^2 v, \tag{58}$$

$$\frac{\partial p}{\partial\tau} = -K\,\frac{\partial\phi}{\partial\widetilde{y}} - \Gamma\boldsymbol{\nabla}_\parallel v - \{\phi,p\} + \chi_\perp\nabla_\perp^2 p + \chi_\parallel\nabla_\parallel^2 p. \tag{59}$$

An example of the turbulent fields created by this system is shown in Fig. 9. In this case $K = 3, \Gamma = 2, S = 0.3$ and $\mu_\parallel = \chi_\parallel = 1$, $\mu_\perp = \chi_\perp = 0.01$. The variation of the turbulence with the system parameters and the shooting code solutions of the linear eigenvalue problem are thoroughly developed in Hamaguchi and Horton (1990, 1992). The first 3D simulation is found in Horton-Estes-Biskamp (1980).

Examining the convection in Fig. 9 shows that the saturation level is such that the convection around the vortical structure is completed within the correlation time τ_c of the field. This is a $\widetilde{\phi}$-level such that the $\mathbf{E}\times\mathbf{B}$-rotation number $R_E = \Omega_E/\Delta\omega \gtrsim 1$ where $\Omega_E = \mathbf{k}\cdot\mathbf{v}_E \sim k_x k_y c/\widetilde{\phi}/B$. The time $2\pi/\Omega_E$ can also be understood by computing the time to convect around the rectangular cell given by $\lambda_x/|v_x| + \lambda_y/|v_y| = 2\pi/k_x k_y(c/\widetilde{\phi}/B)$. As shown earlier, the nonlinear self-binding becomes effective for $R_E > R_{\rm crit} \gtrsim 1$. Thus, this particular saturated state is just into the nonlinear self-binding regime.

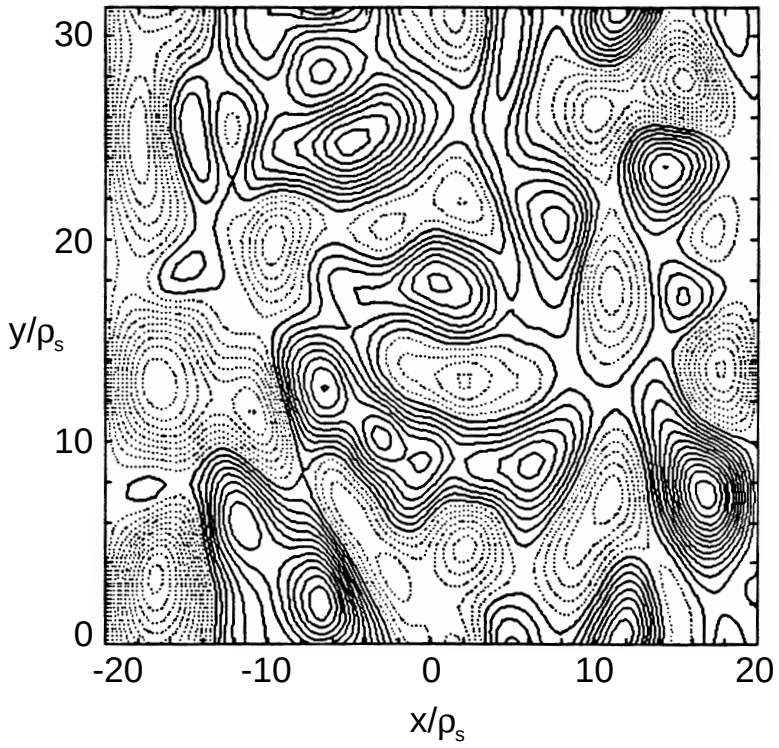

Figure 9: The isopotential contours in the saturated state of a 3D simulation of the ITG equations. Size of the convective cells is $\simeq 6\rho_s$ only slightly larger than $\pi/k_y^{\max}$ for maximizing the linear growth rate. The $\mathbf{E} \times \mathbf{B}$ rotation rate $\Omega_E \simeq 0.9\ [c_s/L_n]$ larger than the maximum growth rate and wave frequency by a factor of 1.5.

The saturation level $R_E = 1$ may also be understood as the level where the mean-square fluctuating pressure gradient just balances the ambient background gradient driven by the auxiliary heating. This level is called the mixing length level and is the standard methods of calculating the turbulence level driven by ambient gradients.

For a given amplitude level of the fluctuations the convective transport depends on the phase relation between δn or δp_i and $\delta\phi$ as discussed in Sec. 1.1. As the rotation number R_E becomes appreciably larger than unity the pressure fluctuation becomes aligned with ϕ: $\delta p_i \approx f(\phi)$ and there is only transport across the separatrices between the trapped regions (Ottaviani, 1997). For $R_E < 1$, however, the phase relation remains not too far from the linear relation between δp_i and ϕ. Thus, quasilinear calculations for the convective flux are typical with the linear $\delta p_i/\delta\phi$-formula used for calculating the phase relations.

In the simulations the effective diffusivity χ_i is defined by

$$\chi_i = \frac{\overline{\langle \widetilde{p}_i \widetilde{v}_{ir} \rangle}}{-p'_{i0}} = \frac{\rho_s}{L_n}\left(\frac{cT_e}{eB}\right)\overline{\left\langle p\,\frac{\partial\phi}{\partial y}\right\rangle}K^{-1}. \tag{60}$$

Here the

$$\overline{g(t)} = \lim_{T\to\infty}\frac{1}{T}\int_0^T g(t)dt$$

and

$$\langle f\rangle = \frac{1}{\Delta L_y L_z}\int_{-L_x}^{L_x} d\widetilde{x}\int_0^{L_y} d\widetilde{y}\int_0^{L_z} d\widetilde{z},\ f(\mathbf{x}) \tag{61}$$

where Δ denotes the width of the region of appreciable turbulence, i.e. the "support" of a function $f(x)$ for homogeneous turbulence $\Delta \to 2L_x$. Figure 10 shows a typical result for the temperature gradient dependence of χ_i in the units of the gyro-Bohm diffusivity $\chi_{gB} = (\rho_s/L_n)(cT_e/eB)$ for the model in Eqs. (57)–(59) and for the parameters given above.

The energy integral E_T for system (57)–(59) is

$$E_T = \frac{1}{2}\int_\Omega d^3x\left[\phi^2 + (\nabla\phi)^2 + v^2 + \frac{1}{\Gamma}\,p^2\right].$$

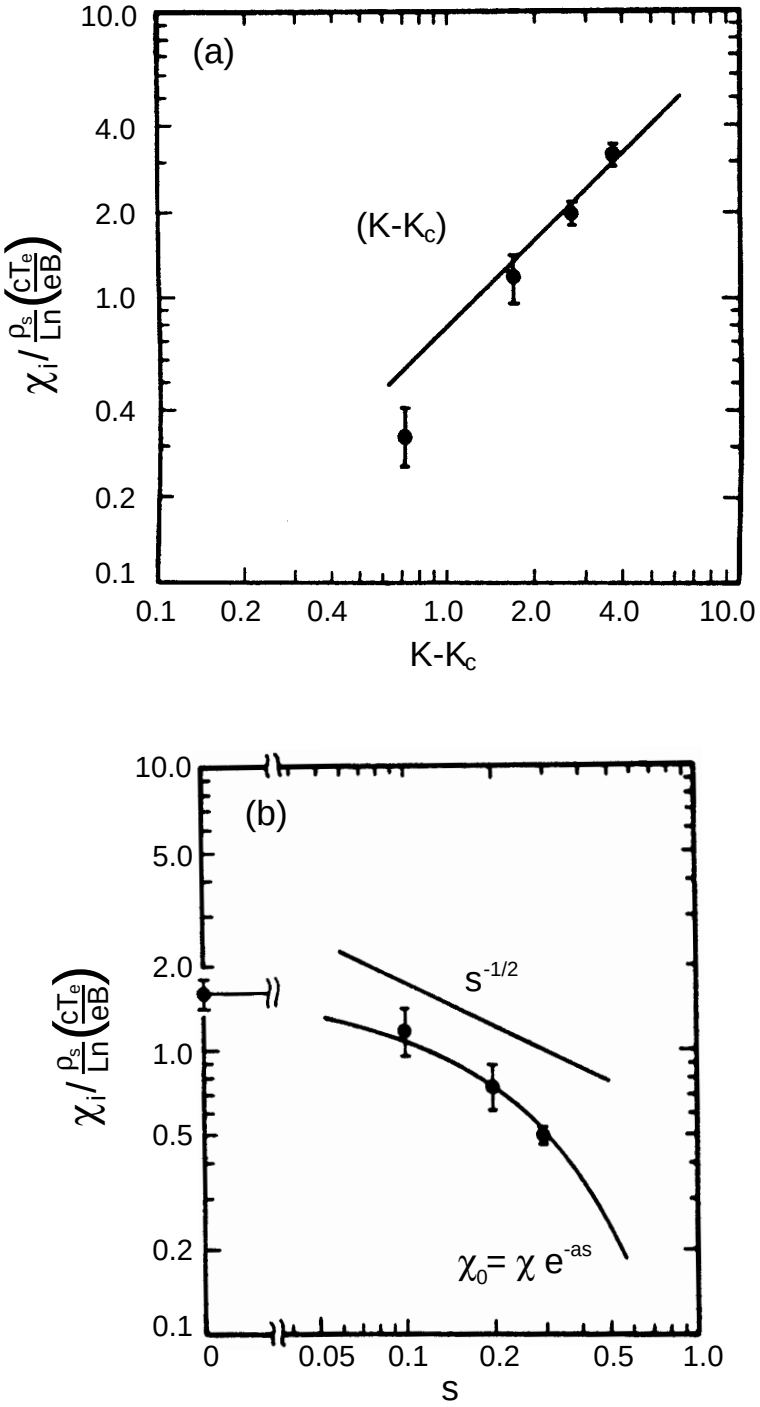

Figure 10: The turbulent ion thermal conductivity in units of the gyroBohm conductivity as a function of the deviation from the critical adiabatic gradient. (a) Increase of thermal conductivity with deviation from the critical ion temperature gradient $K_c = 1.3$ for fixed magnetic shear $S = L_n/L_s = 0.1$ and adiabatic gas constant $\Gamma = 2$. The dots are from steady state averages in the 3D simulation and the heavy line proportional to $K - K_c$ from bifurcation theory; (b) Decrease of the thermal diffusivity with increasing magnetic shear S for fixed temperature gradient $K = 3$ with other parameters the same as in (a).

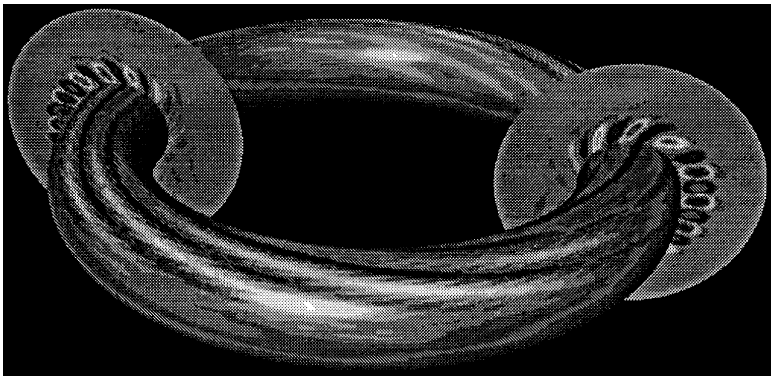

Figure 11: The linear phase of a global ITG mode in a tokamak obtained by the Parker group as part of the fusion Grand Challenge Supercomputer project. The method used is an extension to guiding centers of the classical particle-in-cell simulation technique.

Similar to Eq. (47) for the barotropic instability before the hydrostatic equilibrium approximation is used. The power transfer fluxes between the three energy components are $\left\langle v\nabla_{\parallel}\phi\right\rangle, \left\langle p\nabla_{\parallel}v\right\rangle$ and $Q = -\left\langle p\partial_y\phi\right\rangle$ with rate of change of the total energy given by

$$\frac{dE_T}{dt} = \frac{KQ}{\Gamma} - \sum_{\alpha=1}^{5} P_\alpha$$

where P_α are the positive definite dissipation integrals $\mu_\perp \left\langle(\nabla^2\phi)^2\right\rangle$, $\mu_\perp \left\langle(\nabla_\perp v)^2\right\rangle, \mu_{\parallel}\left\langle(\nabla_{\parallel}v)^2\right\rangle$, $\chi_\perp \left\langle(\nabla_\perp p)^2\right\rangle$ and $\chi_{\parallel}\left\langle(\nabla_{\parallel}p)^2\right\rangle$. In the turbulent steady state the thermal flux Q times the temperature gradient K balances the viscous-thermal diffusive dissipation.

Since the time of this work (Hamaguchi and Horton, 1990) the ITG modeling has received much attention due to its almost unique ability to explain the power balance in the large fusion confinement devices. Now much more sophisticated fluid descriptions called gyrofluids using up to 13 pdes are used to describe the turbulence. The turbulence was also chosen as the topic for the fusion Grand Challenge project in super computing. In this project large particle simulation codes in the full 3D torus are used for the simulations of drift wave turbulence. A typical result is shown in Fig. 11 from Parker *et al.* (1996). Waltz *et al.* (1994) gives a comprehensive analysis with the gyro-Landau equations and compares the results with three discharges from TFTR.

3 Thermal Balance in the Atmosphere

Solar energy is the primary source of atmospheric heating. Other thermal sources from the upper mantle and dissipation of ionospheric currents are negligible in comparison. Of the total solar power intercepted by the Earth, about 40% is estimated to be reflected back into space and the remaining power $P_0 \cong 10^{17}\,\mathrm{W}$ is preferentially absorbed in the equatorial zone where angle of incidence is normal. The distribution of the absorbed solar power is about 27% into the atmosphere and 73% into the ocean and land (Gill, 1982, p. 10). The atmosphere and the oceans each transport northward from the equitorial region a power of about $3 \times 10^{15}\,\mathrm{W}$. For comparison the power dissipated by ionospheric currents reaches $10^{12}\,\mathrm{W}$ during magnetic substorms that occur on average every few hours (Horton and Doxas, 1997). The result is a substantial temperature gradient between the equatorial zone and the polar regions which derives atmospheric zonal flows and large three-dimensional convection cells. The atmospheric turbulence is divided into large space scale-long-time scale synoptic motions ($L \sim \rho_R > 1000\,\mathrm{km}, \Delta t > 1/f \sim 1\,\mathrm{day}$) and smaller scale-faster motions for which the gradient of the Ciriolos parameter $\beta = \partial f/\partial y$ is not important. The large scale motions are directly analogous to the low frequency drift instabilities of the magnetized plasma. The role of the baroclinic instability driven by the horizontal temperature gradient $\partial T/\partial y$ is the analog of the ion temperature gradient instability in plasma. Thus, it is important to compare the role of turbulent thermal convection in the two systems.

We now estimate the thermal diffusivity χ implied by the solar input power to the equatorial atmosphere and the meridional temperature gradient showing that the result is consistent with corresponding plasma thermal diffusivity formulas used in magnetic fusion research. In plasma confinement studies there are two forms of the thermal diffusivity scaling (gH/f and $(gH)^{3/2}/f^2R_p$) in plasma confinement studies called Bohm and gyro-Bohm, respectively, that are currently used. The gyro-Bohm is the formula shown in Fig. 10. In the Bohm scaling the

system is near the critical gradient for convection so that there is a small coefficient in the Bohm formula. For the drift wave or gyro-Bohm, thermal diffusivity formula the coefficient is order unity.

In terms of the atmospheric parameters these two thermal diffusivity formulas are $\chi_B = 5 \times 10^{-3}(gH/f)$ and $\chi_{gB} = 0.3(\rho_R/R_p)(gH/f) = 0.3(gH)^{3/2}/R_p f^2$ respectively. Let us take $(gH)^{1/2} = 300\,\mathrm{m/s}$ and $f = 7.3 \times 10^{-5}/\mathrm{s}$ and the planetary radius $R_p = 6 \times 10^6\,\mathrm{m}$. These formulas give $\chi_B = 10^6\,\mathrm{m}^2/\mathrm{s}$ and $\chi_{gB} = 1.5 \times 10^7\,\mathrm{m}^2/\mathrm{s}$. The small coefficient in the Bohm formula is interpreted to express the fact that the large scale convective cells $L = (\rho_R R_p)^{1/2}$ observed in the global simulations force the temperature profile to relax, keeping the system close to marginal stability.

The empirical case for the Bohm transport model is presented in Erba *et al.* (1995) for discharges up to 7 MA of plasma current. The stored plasma thermal energy is approximately $10^6\,\mathrm{J}$ with power flux through the plasma of order $20\ \mathrm{MW}/80\,\mathrm{m}^2 \cong 2 \times 10^5\,\mathrm{W/m}^2$. The thermal energy confinement (storage) times is $\tau_E = E/P \cong 0.5\,\mathrm{s}$. The ion thermal diffusivity χ_i is approximately three times the electron χ_e.

In the drift wave (gyro-Bohm) formula the system is in a state of well-developed turbulence (well away from marginal stability) with the horizontal scales $L \simeq 4\rho_R$ and the correlation time $\tau_c = 1/\max(\omega_k) \simeq 5R_p/\sqrt{gH}$ corresponding to the maximum wave frequency at $k_\perp \rho_R = 1$. Correlation times of this order correspond to a few days.

3.1 Power balance in the atmosphere

The energy content of the atmosphere is divided into thermal energy $E_p = (5/2)nk_BT$ and mean kinetic energy $E_{\mathbf{k}}$. The kinetic energy is divided into mean zonal flows $\overline{E}_k$ and turbulent flows $\widetilde{E}_k$. We calculate for the energies $E_p = 10^{24}\,\mathrm{J}$, $\overline{E}_{\mathbf{k}} = 10^{21}\mathrm{J}$ and $\widetilde{E}_{\mathbf{k}} = 10^{20}\mathrm{J}$. Monin (1972) considers the confinement time for the energy $E_{\mathbf{k}}$ arguing that 2% of the absorbed solar power $P_s = 10^{17}\,\mathrm{W}$ is converted into kinetic energy $E_{\mathbf{k}} = 10^{21}\,\mathrm{J}$ giving

$\tau = E_{\mathbf{k}}/2 \times 10^{15}\,\mathrm{W} = 5 \times 10^5\,\mathrm{s} \cong 1$ week. Monin notes that this decay time is consistent with the Richardson's four-thirds law $\nu_L = \varepsilon^{1/2} L^{4/3}$ for the $\widetilde{E}_k = 5 \times 10^{20}\,\mathrm{J}$. The turbulent viscosity ν_L is compared with the turbulent thermal diffusivity in the following subsection.

The thermal flux from the equatorial zones to the polar regions is

$$F = -n\chi \frac{dT}{dy} \simeq \frac{n\chi \Delta T}{R_E} = 3 \times 10^{15}\,\mathrm{W} \Big/ \left[1.3 \times 10^{11}\,\mathrm{m}^2\right] = 2 \times 10^4\,\mathrm{W/m}^2 \tag{62}$$

where we require for steady state that the flux F times the cross-sectional area $A = 2\pi R_E \cos\theta_L\, H$ at the latitude $\theta_L = 50^\circ$ equals the fraction of the solar input power $3 \times 10^{15}\,\mathrm{W}$ that is transported northward through the atmosphere (Gill, 1982, p. 15) to the arctic region. Equation (62) introduces the definition of the effective thermal diffusivity χ due to the turbulent convection. Taking the equator-polar temperature gradient as $\Delta T/R_E = 10^\circ\mathrm{C}/6 \times 10^6\,\mathrm{m}$, we infer the mean turbulent diffusivity from Eq. (62) is

$$\chi_{\mathrm{PB}} = 3 \times 10^7\,\mathrm{m}^2/\mathrm{s} \tag{63}$$

for steady-state power balance (PB). This power balance thermal conductivity is approximately two times the standard plasma physics analogs for temperature gradient driven thermal diffusivities estimated above for χ_{gB}.

3.2 Anomalous viscosity and the turbulent Prandtl number

The thermal diffusivity (63) may be compared to the large scale turbulent viscosity ν_L. Monin (1972) gives that $\nu_L = 10^7\,\mathrm{m}^2/\mathrm{s}$ at the scale $L = 2200\,\mathrm{km}$. Using this value for the turbulent viscosity and Eq. (63) for the turbulent thermal diffusivity gives the effective Prandtl number of $\nu_L/\chi = 1/3$. To extrapolate ν_L at $L = 2200\,\mathrm{km}$ to $L = R_E = 6340\,\mathrm{km}$ using the Richardson four-thirds law would increase the turbulent viscosity to $\nu_L = 10^7\,\mathrm{m}^2/\mathrm{s}(6340/2200)^{4/3} = 4 \times 10^7\,\mathrm{m}^2/\mathrm{s}$ making the effective Prandtl number close to unity.

The effective viscosity also follows from the Kolmogorov eddy lifetime. Monin, citing Palmén (1961), estimates the Kolmogorov energy injection constant $\varepsilon = 4\,\mathrm{cm}^2/s^3$ using 2%

of the solar input power as driving the turbulent convection. This value of ε is close to that of Brunt (1926) $\varepsilon = 5\,\mathrm{cm}^2/s^3$ based on independent arguments.

In conclusion, the turbulent diffusivity of thermal energy from the equator to the poles is of the same order as the turbulent eddy viscosity. The same situation is found in toroidal plasmas where the toroidal flow velocities of order a $100 - 300\,\mathrm{km/s}$ are known to decay with a turbulent viscosity ν_ϕ that is approximately $2/3\,\chi$ where χ is the thermal diffusivity from the temperature gradient driven turbulence (Sugama and Horton, 1997). The reason that the Prandtl number for the large scale fluctuations is order unity for both the plasma and the geophysical fluid is that the mechanism for the transport of both the momentum and the thermal energy is the large scale geostrophic $\mathbf{E} \times \mathbf{B}$ horizontal turbulent flows.

Acknowledgments

The author wishes to express his thanks to R.L. Dewar and R.W. Griffiths for the timely gathering of researchers in the field of geophysical fluid dynamics and plasma turbulence. Useful discussions with many workshop participants including B. Blackwell, G. Holland, M. Nezlin, V. Naulin, R. Kinney, and M. Wakatani are acknowledged. This work was supported by the U.S. Dept. of Energy Contract # DE–FG03–96ER–54346.

References

[1] Brower, D.L., Peebles, W.A., Kim, S.K., Luhmann, Jr., N.C., Tang, W.M., and Phillips, P.E., *Phys. Rev. Lett.* **54**, 689 (1987).

[2] Brower, D.L., Redi, M.H., Tang, W.M., Bravenec, R.V. *et al.*, *Nucl. Fusion* **29**, 1247 (1989).

[3] Brunt, D., *Physical and Dynamical Meteorology*, 2nd ed., Cambridge Univ. Press, New York, 1939.

[4] Chandrasekhar, S., *Hydrodynamic and Hydromagnetic Stability*, Dover Publications, Inc., New York, 1961.

[5] Charney, J.G., *Geofys. Publikasjoner, Norske Videnskaps-Akad. Oslo* **17**, 17 (1948).

[6] Erba, M., Parail, V., Springman, E., and Taroni, A., *Plasma Phys. Control. Fusion* **37**, 1249 (1995).

[7] Gill, A.E., *Atmosphere–Ocean Dynamics*, Academic Press, London, 1982.

[8] Griffiths, R.W., and Hopfinger, E.J., *J. Fluid Mech.* **173**, 501 (1986).

[9] Griffiths, R.W., and Hopfinger, E.J., *J. Fluid Mech.* **178**, 73 (1987).

[10] Hamaguchi, S., and Horton, W., *Phys. Fluids B* **2**, 1833 (1990).

[11] Hamaguchi, S., and Horton, W., *Phys. Fluids B* **4**, 319 (1992).

[12] Hasegawa, A., and Mima, K., *Phys. Rev. Lett.* **39**, 205 (1977) and *Phys. Fluids* **21**, 87 (1978).

[13] Hasegawa, A., Maclennan, C.G., and Kodama, Y., *Phys. Fluids* **22**, 2122 (1979).

[14] Hazeltine, R.D., and Meiss, J.D., *Plasma Confinement*, Addison-Wesley, Redwood City, California, 1992.

[15] Hobson, D.D., *Phys. Fluids A* **3**, 3027–3033 (1991).

[16] Holland, G.J., *Meteorol. Atmos. Phys.* **56**, 57–79 (1995).

[17] Horton, W., Estes, R., and Biskamp, D., *Plasma Phys.* **22**, 663 (1980).

[18] Horton, W., Choi, D.-I., and Tang, W.M., *Phys. Fluids* **24**, 1077 (1981).

[19] Horton, W., Lindberg, D., Kim, J-Y., Dong, J.-Q., Hammett, G.W., Scott, S.D., Zarnstorff, M.C., and Hamaguchi, S., *Phys. Fluids B* **4**, 953 (1992).

[20] Horton, W., and Petviashvili, V., eds. Horton, W., Ichikawa, Y., Prigogine, I. (Ed. in-Chief), Zaslavsky, G., "On the trapping condition for planetary vortex structures," *Research Trends in Physics: Chaotic Dynamics and Transport in Fluids and Plasmas*, American Institute of Physics, New York, 1993.

[21] Horton, W., and Ichikawa, Y.-H., *Chaos and Structures in Nonlinear Plasmas*, World Scientific, 1996, chap. 6, pp. 221–273.

[22] Horton, W., and Doxas, I., *J. Geophys. Res.* **102**, (Dec. (1997), and **101**, 27223 (1996).

[23] Jovanović, D., and Horton, W., *Phys. Fluids B* **5**, 9 (1993).

[24] Kim, J-Y., and Horton, W., *Phys. Fluids B* **3**, 1167 (1991).

[25] Kono, M., and Horton, W., *Phys. Fluids B* **3**, 3255–3262 (1991).

[26] Laedke, E.W., and Spatschek, K.H., *Phys. Fluids* **29**, 133–142 (1986).

[27] Laedke, E.W., and Spatschek, K.H., *Phys. Fluids* **31**, 1492 (1988).

[28] Larichev, V.D., and Reznik, G.K., *Fiz. Plasmy* **3**, 270 (1976).

[29] Meiss, J.D., and Horton, W., Jr., *Phys. Fluids* **26**, 990 (1983).

[30] Monin, A.S., *Weather Forecasting as a Problem in Physics*, MIT Press, 1972.

[31] Muzylev, S.V., and Reznik, G.M. *Phys. Fluids B* **4**, 2841 (1992).

[32] Nezlin, M.V., and Snezhkin, E.N., in *Rossby Vortices, Spiral Structures, Solitons*, Springer-Verlag, 1993, pp. 196–203.

[33] Nycander, J., *Phys. Fluids A* **4**, 467–476 (1992).

[34] Ottaviani, M., Beer, M.A., Cowley, S.C., Horton, W., and Krommes, J.A., *Phys. Rep.* **283**, 121–146 (1997).

[35] Palmén, E., *Geofis. Pura Appl.* **49**, 167 (1961).

[36] Parker, S.E., Mynick, H.E., Artun, M., Cummings, J.C., *et al.*, *Phys. Plasmas* **3**, 1959 (1996).

[37] Pedlosky, J., 1987, *Geophysical Fluid Dynamics*, Springer-Verlag, New York, pp. 518–532.

[38] Petviashvili, V.I., *Fiz. Plazmy* **3**, 270 [Sov. *J. Plasma Phys.* **3**, 150 (1977).

[39] Rossby, C.G., in *The Atmospheres of the Earth and Planets*, Univ. of Chicago Press, Chicago, 1948, p. 25.

[40] Sakuma, H., and Ghil, M., *Phys. Fluids A* **3**, 408–414 (1991).

[41] Su, X.N., Horton, W., and Morrison, P.J., *Phys. Fluids B* **3**, 921 (1991).

[42] Su, X.N., Horton, W., and Morrison, P.J., *Phys. Fluids B* **4**, 1238 (1992).

[43] Scott, S.D., Barnes, Cris W., Ernst, D., Schivell, J., Synakowski, E.J., Bell, M.G., Bell, R.E., Bush, C.E., Fredrickson, E.D., Grek, B., Hill, K.W., Janos, A., Jassby, D.L., Johnson, D., Mansfield, D.K., Owens, D.K., Park, H., Ramsey, A.T., Stratton, B.C., Thompson, M., and Zarnstorff, M.C., "Parametric Variations of Ion Transport in TFTR," in *U.S.-Japan Workshop on Ion Temperature Gradient-Driven Turbulent Transport*, AIP Conference Proceedings, Austin, TX, 1993.

[44] Sugama, H., and Horton, W., *Phys. Plasmas* **4**, 405 (1997).

[45] Swaters, G.E., *Phys. Fluids* **29**, 1419–1422 (1986).

[46] Tasso, H., *Phys. Lett. A* **24**, 618 (1967).

[47] Waltz, R.E., Kerbel, G.D., and Milovich, J., *Phys. Plasmas* **1**, 2229 (1994).